THREE LECTURES ON BARYON RESONANCES

M. Ferro-Luzzi

CERN
Geneva

Table of Contents

First Lecture

Second Lecture

Third Lecture

- o 0 o -

THREE LECTURES ON BARYON RESONANCES

M. Ferro-Luzzi,
Track Chambers Division,
CERN,
Geneva, Switzerland.

FIRST LECTURE

I. Introduction

Avowed purpose of this school is to give a theoretical background to young experimentalists. So, I don't know where the baryon resonances come in. The art here is mainly at an experimental stage and the best thing that most people could learn is how to deal with the experimental data. Still, in order to comply with the above purpose, I will try to skip all or almost all of the experimental details and concentrate on what remains: the results and their meaning. Theoretical interpretations of baryon resonances as such, particularly when it comes to quantitative predictions, are rather skimpy. Detailed calculations do not exist and the predictions of the various symmetry schemes are somewhat flexible. The reason for all this is probably that much more information has to be put together on the experimental side before realistic calculations can be performed. What remains, then, and what I will try to present here, is a phenomenological description of these resonances and some general recipe on how they can be studied. The emphasis will be on methods rather than on systematics. Special cases will be discussed only when illustrative of a certain procedure. Although the bibliography will contain as much as possible of the relevant literature, these lectures have no pretence of offering an updated review of baryon resonances. Examples of the latter do come out regularly once a year and those interested are referred to them. Finally, I should mention that most of the examples and approaches discussed are related to the work of the CHS group[1] during these last few years and should not be taken as the most objective and unbiased view of the subject.

Since there are only three lectures, the best approach is to start as quickly as possible. The plan of the lectures can be understood from the table of contents. The first subject to be treated will be the hyperon resonances; along with them, the basic definitions and necessary formalism will be recalled.

II. Production and formation experiments

I suppose that everybody here is already familiar with the quantum numbers of the elementary and not-so-elementary particles. For those who aren't, the Rosenfeld tables[2] will provide an exhaustive collection of such and other numbers. Hyperon resonances have in common a baryon number $B = 1$ and a strangeness S different from zero. Convenient historical symbols[3] are Λ for $S = -1$ and isotopic spin $I = 0$, Σ for $S = -1$ and $I = 1$, Ξ for $S = -2$ and $I = 1/2$, Ω for $S = -3$ and $I = 0$. A generic symbol Y^* is also frequently used to denote any hyperon resonance. Additional conventions do exist, identifying the angular momentum J and parity P of the particles,[3] but their usefulness is strongly limited by the very lack of knowledge existing in many cases about those numbers.

There are many possible ways of presenting the known hyperon resonances, from a simple table of masses to a sophisticated (and often unwarranted) collection of SU(3) multiplets perhaps even arranged along Regge-trajectories. In fig. 1 the representation chosen[4] has the advantage of exhibiting the most relevant experimental features while avoiding any specific theoretical point of view. All reasonably well established $S = -1$ resonances are here plotted on a "mass" versus "J^P" diagram. When the latter quantity is not known, a vertical line replaces the point. Open circles indicate uncertainty in J^P attribution or resonance existence. The horizontal bars indicate the full width Γ of the resonances. Only Λ and Σ type of resonances are shown, no other types being known at present.

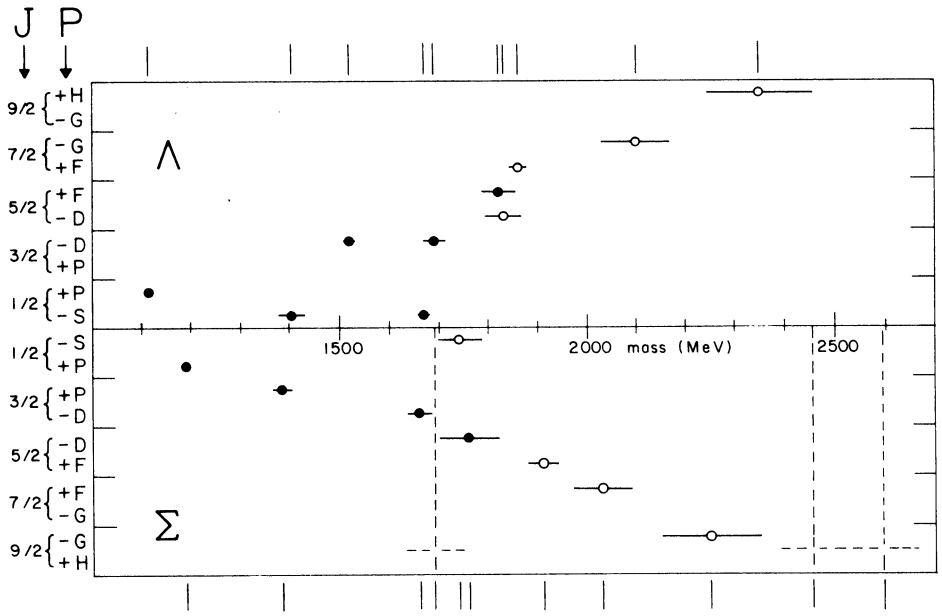

Fig. 1

The following features are worth digressing on:

a) Points and lines are crowded towards low masses; it looks like resonances fade away with increasing mass. This is a simple reflection of the fact that the low mass region has been studied first and more thoroughly. A few years ago the whole map would have been just as unpopulated as its present high mass region.

b) The values of J seem to increase with mass. Perhaps some physical reality hides behind this. Still, it is a fact that resonances with high J are more easy to detect, particularly at high energy.

c) The width also becomes larger with increasing mass. Here again one should keep in mind that a good energy resolution, such as is necessary in order to detect narrow resonances, is increasingly lacking when going up in energy.

Let us now quickly review the methods and techniques for finding and studying these resonances. Figs. 2 and 3 show two examples of what is known as a "production" type of experiment: the oldest[5] and one of the most recent[6], respectively. The general procedure consists of investigating

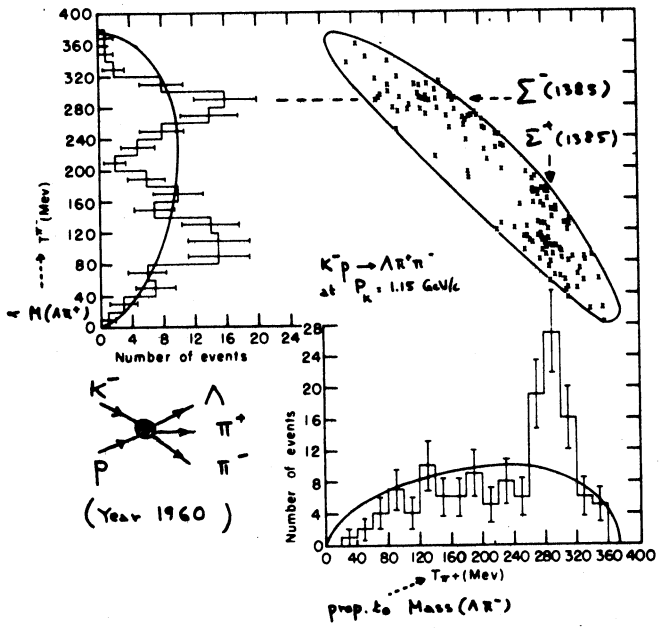
Σ⁻(1385)
Σ⁺(1385)
K⁻p → Λπ⁺π⁻
at P_K = 1.15 GeV/c
Number of events
K⁻
Λ
π⁺
p
π⁻
(Year 1960)
Number of events
T_π+(Mev)
prop. to Mass (Λπ⁻)

Fig. 2

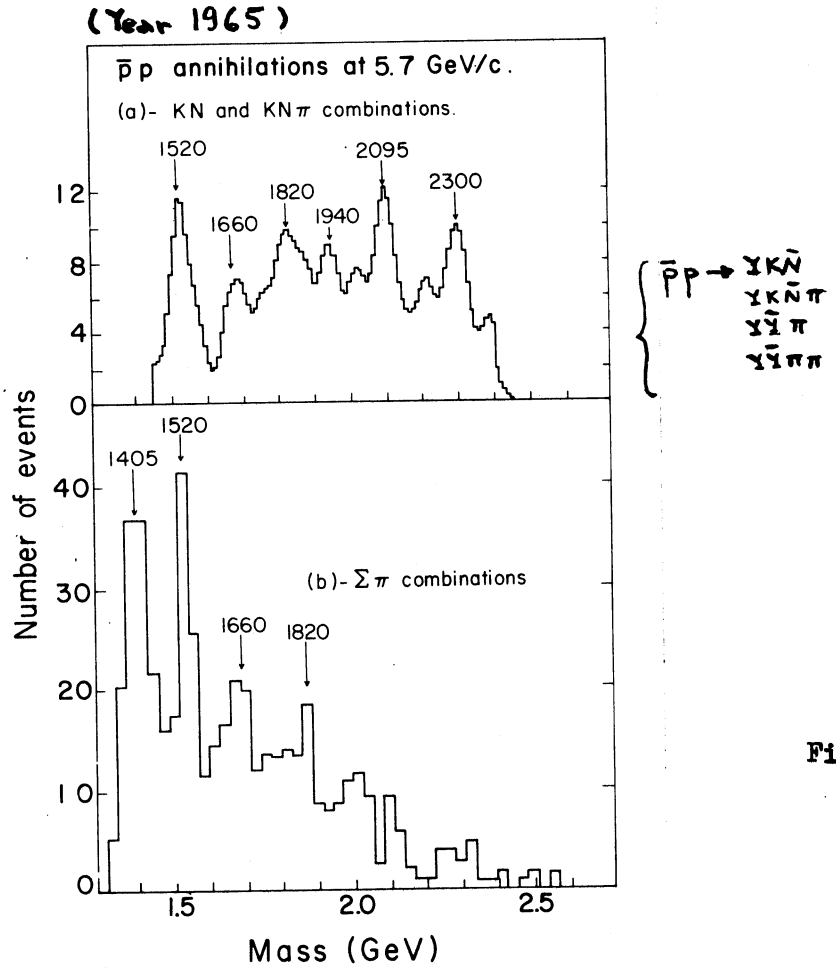
(Year 1965)
p̄p annihilations at 5.7 GeV/c.
(a)- KN and KNπ combinations.
1520
1660
1820
1940
2095
2300
(b)- Σπ combinations
1405
1520
1660
1820
Number of events
Mass (GeV)
p̄p → ΥKN̄
ΥKN̄π
ΥῩπ
ΥῩππ

Fig. 3

the spectrum of effective mass of two (fig. 2) or more particles (fig. 3) emitted in certain reactions. All enhancement not explainable in terms of kinematics (for example "phase-space") or statistical fluctuations is assumed to come from the decay of a resonance, its height being related to the production rate and its mass spread to its width. Ambiguities in interpretation arise when several resonances are simultaneously produced, as in the overlap region of the plot of fig. 2 and in the more complicated combinations possible for most of the reactions of fig. 3. The sketches of fig. 4 show how a 3-particle final state (the simplest in this type of experiment) can originate from three distinct resonant configurations.

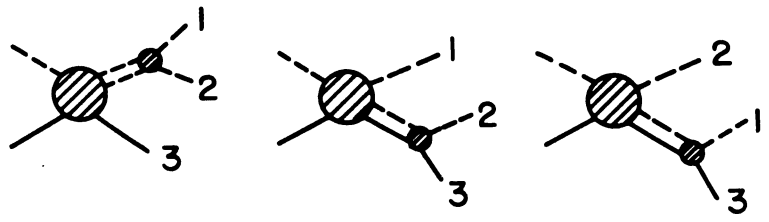

Fig. 4

It is clear from just these examples how anything more than an attribution of mass, width and isospin must heavily depend on specific assumptions on the final state interactions of the particles present, on the production mechanism and other possible effects which are usually far from well understood. This is reflected on the rarity of meaningful J^P determinations achieved through these experiments. Reference 7 discusses in detail the methods devised for measuring spin and parity of resonances "produced" in the above manner. It should be noticed, finally, that, in addition to the above mentioned problems, these types of experiments as performed in practice are usually very much limited by lack of statistics.

The situation of the S = -2 resonances, shown in fig. 5, exemplifies dramatically the difficulties of the "production" experiments; only the latter are indeed available in this case. The resonances are much fewer,

uncertain and little is known about their quantum numbers. The statistical limitations are here much more severe than for the S = -1 case. This can be

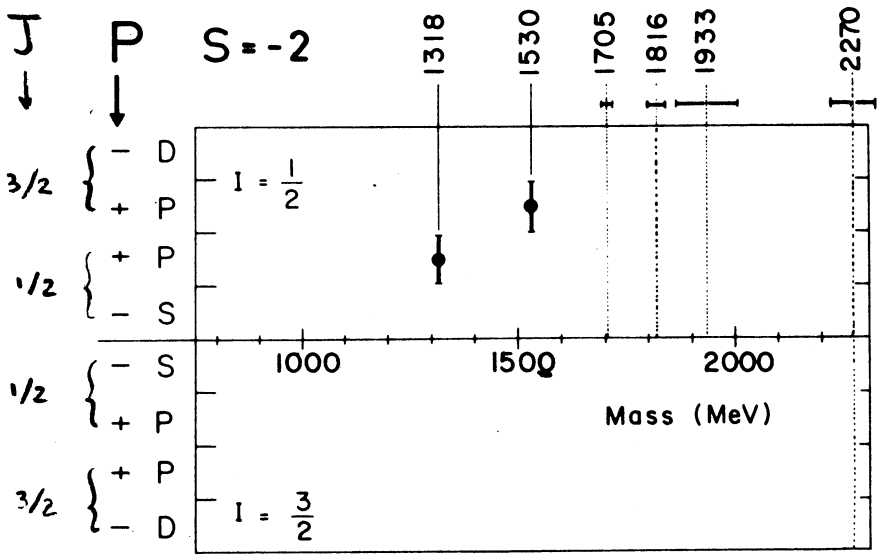

Fig. 5

seen, for example, in the collection of data from a large experiment[8] reproduced in fig. 6. One can imagine, of course, that there is a natural lack of these resonances; still, it may be more likely that the experimental difficulties are such as to hinder both their identification and the determination of their quantum numbers.

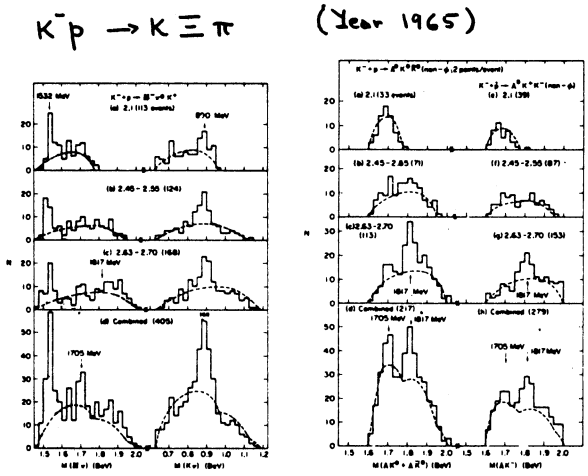

Fig. 6

Turning now to the other possible approach - the one referred to as "formation" - fig 7 shows a schematic parallel between this and the previous approach. The advantage here is that no third partner is around to confuse

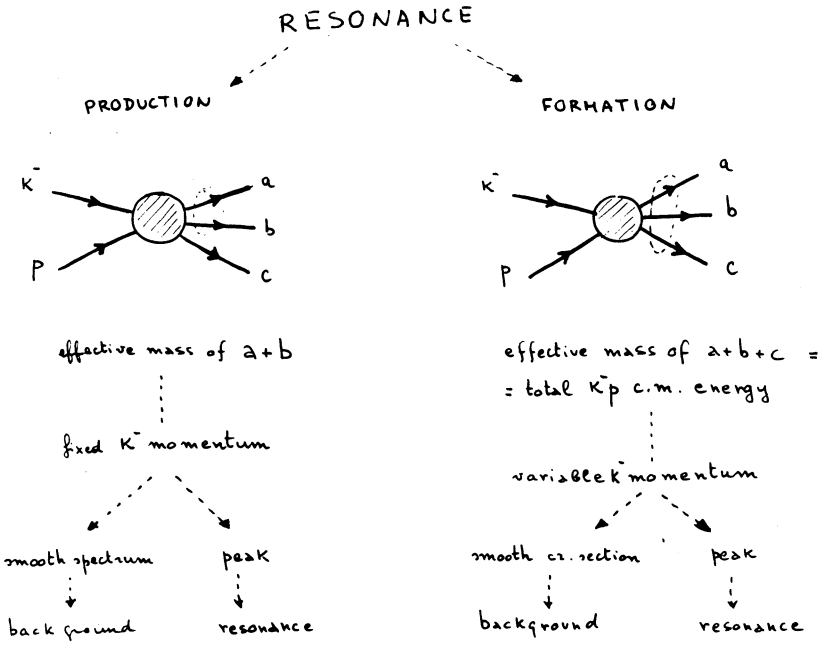

Fig. 7

things; the limitation, that only those resonances which are sufficiently well coupled to the experimental systems used in the "formation" can be studied. Apart from the problems introduced by the "background" (reactions not proceeding through the resonant state), a study of the angular distributions of the final state provides all the information necessary to determine the quantum numbers of the decaying state. Figs. 8 and 9 give two examples, one very early[9], the other more recent[10], of how the formation of resonances may appear in practice. The process in fig. 8 shows one aspect of the formation of $\Lambda(1520)$ via K^-p collisions. The resonance is here seen to decay into the $\Sigma\pi$ mode: $\Sigma^+\pi^-$, $\Sigma^-\pi^+$ and $\Sigma^0\pi^0$. The formation is superposed to a sizeable background of non-resonant processes. The resonance being in a $3/2^-$ state and the background in a predominantly $1/2^-$ state, the change in differential cross section when traversing the resonant energy is quite drastic. A detailed analysis of this change and the related variations in the other

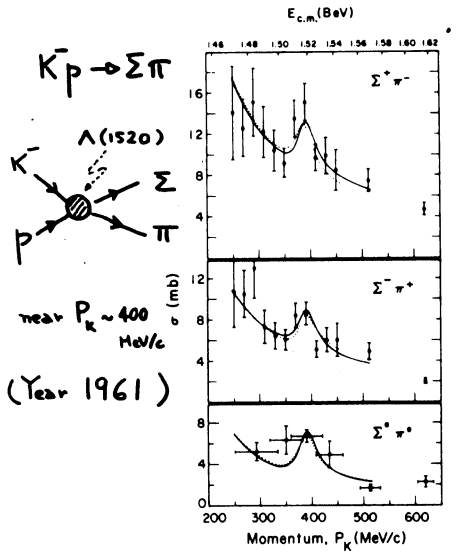

Fig. 8

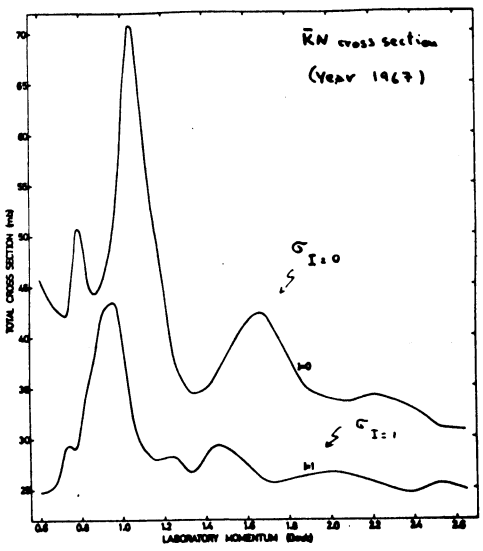

Fig. 9

channels (K^-p, $\bar{K}^0n$, $\Lambda\pi^+\pi^-$) allows a complete identification of the resonance[9]. Although by today's standards the experiment would not be considered as statistically very rich, the information provided was sufficient to pinpoint all the relevant quantum numbers and branching ratios of the resonance. Fig. 9 shows, for a similar situation, how even a simple but accurate measurement of the total $\bar{K}N$ cross section[10] (separated into its two isospin components) can already yield an impressive amount of useful information on resonances whose $\bar{K}N$ branching fraction may be as small as a few percent. Mass, width, isospin and the product $(J + 1/2)x$ where x is the elastic branching fraction (the "elasticity" of the resonance), is the information obtainable through this type of measurements. Any further information, like J^P and branching fraction into different channels, requires additional measurements of the type mentioned in connection with fig. 8.

Before ending this hurried survey of the methods to identify resonances, one more possibility is worth mentioning. It may happen that the decay products of resonances occurring in formation experiments are themselves other resonances which then decay according to their own mode. Fig. 10 shows examples of this mixed "formation - production" behaviour: case (a) has actually been observed[11], (b) is a possibility which for the moment needs more

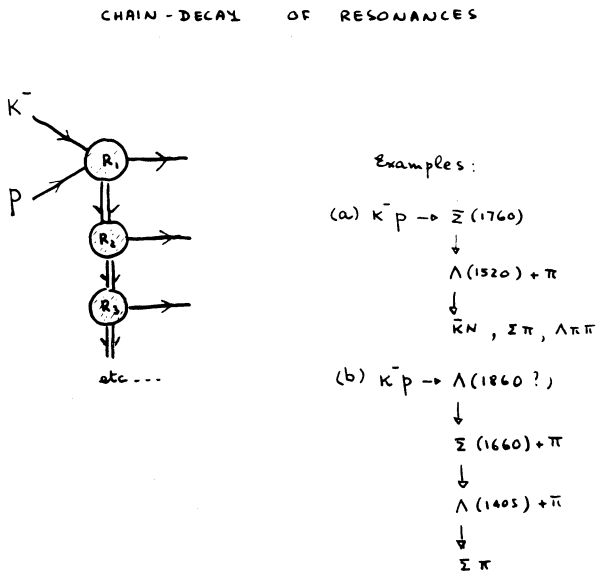

Fig. 10

statistics to be confirmed[12]. Apart from the folkloristic side, these phenomena are quite useful. Angular correlations directly connected with the J^P of the various resonances will be present throughout the decay chain; if the statistics are sufficient and the resonances are well-behaved (widths small, backgrounds low, etc.) then these correlations can be easily exploited to determine the unknown J^P values. This was the case for example (a) of fig. 10, where the known information was the J^P of $\Lambda(1520)$ and the unknown was the J^P of $\Sigma(1760)$. Fig.11 is an excerpt from ref.11 showing the evidence for $\Sigma(1760)$ formation and subsequent decay into $\Lambda(1520)$. A discussion of the angular correlations and the details of the analysis can be found in the above reference.

III. Partial wave decomposition

From now on we shall concentrate on the "formation" type of experiments and, more in general, on what is called a "partial wave analysis". A brief review of the most relevant formulae connected with this analysis is in order first, so as to lay the ground for the next lecture. In an accelerated

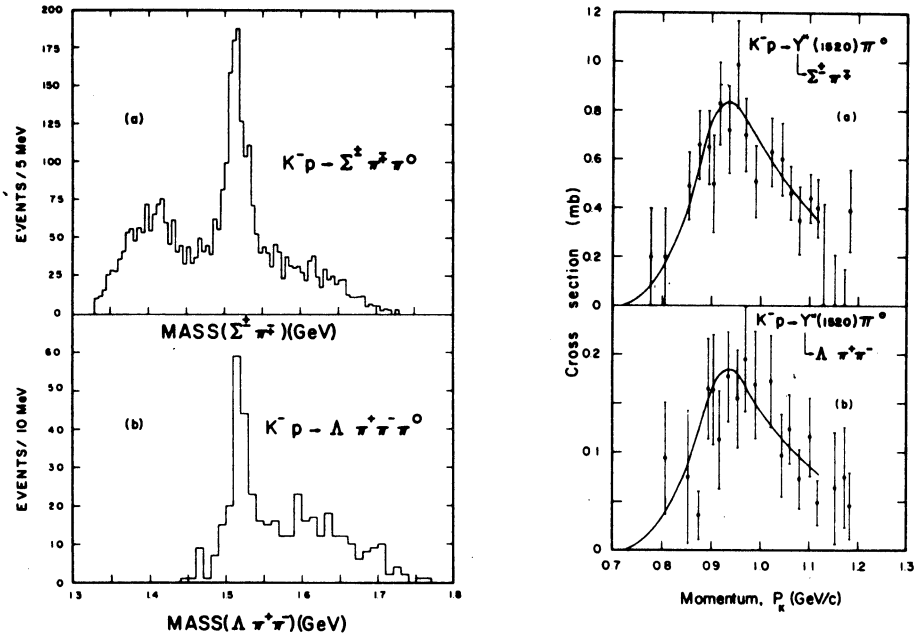

Fig. 11

course such as this there is clearly no time to go into derivations or comprehensive discussions of the formalism outlined below. I will simply list the main results and will convey a visual impression of how and from where they come out. Full treatments can be found practically in any of the available textbooks or lecture notes (see, for example, refs. 4 and 13).

Referring first to the simpler case of a spinless particle incident on a spinless target, figs. 12 to 14 recall how the incident beam can be thought of as a plane wave, how the latter can be expanded into an infinite sum of spherical waves corresponding to all possible values of the orbital angular momentum ℓ, how the effect of the target can be represented by a "phase shift" and an "absorption" of the outgoing spherical waves, how finally the scattered wave can be factorized into a radial term and a term depending only on the scattering angle ϑ. The latter is called "scattering amplitude" and its components are products of Legendre polynomials $P_\ell(\cos\vartheta)$ times complex numbers called "partial wave amplitudes". It is the knowledge of these partial waves which is sought in the analyses discussed in the next lecture.

BEAM OF PARTICLES INCIDENT ON A SPINLESS TARGET.

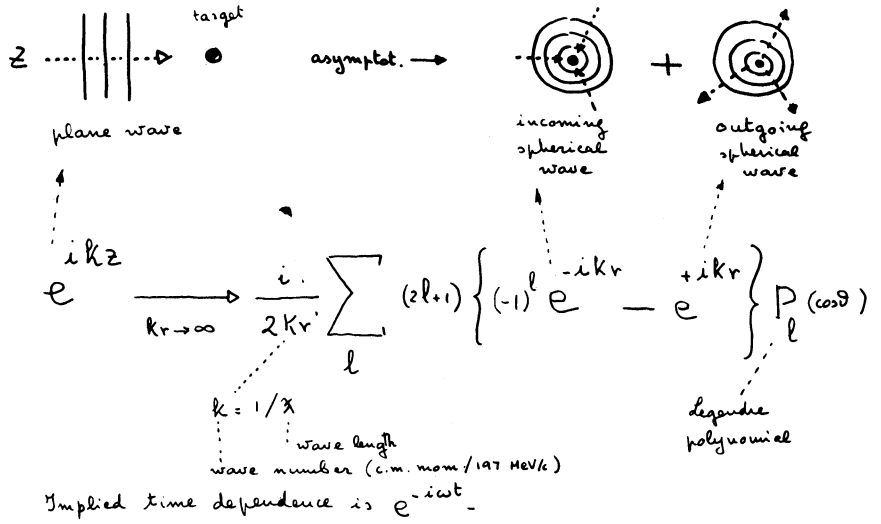

Fig. 12

The effect of the target is only on the outgoing spherical wave:

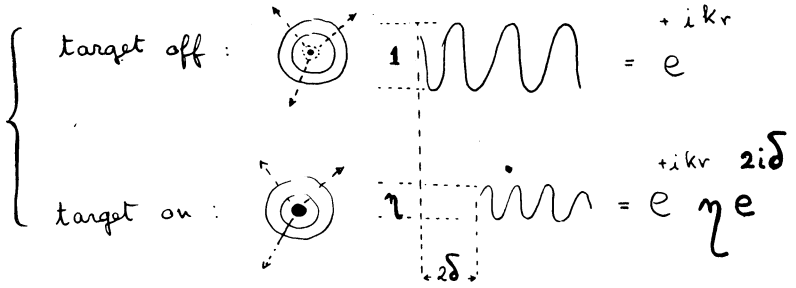

η : absorption parameter

δ : phase shift

All this depends on l, of course

if η is 1, there is no absorption = all particles coming in do also come out.

if δ is 0 there is no scattering = beam is undisturbed.

and $\eta = 1$

Fig. 13

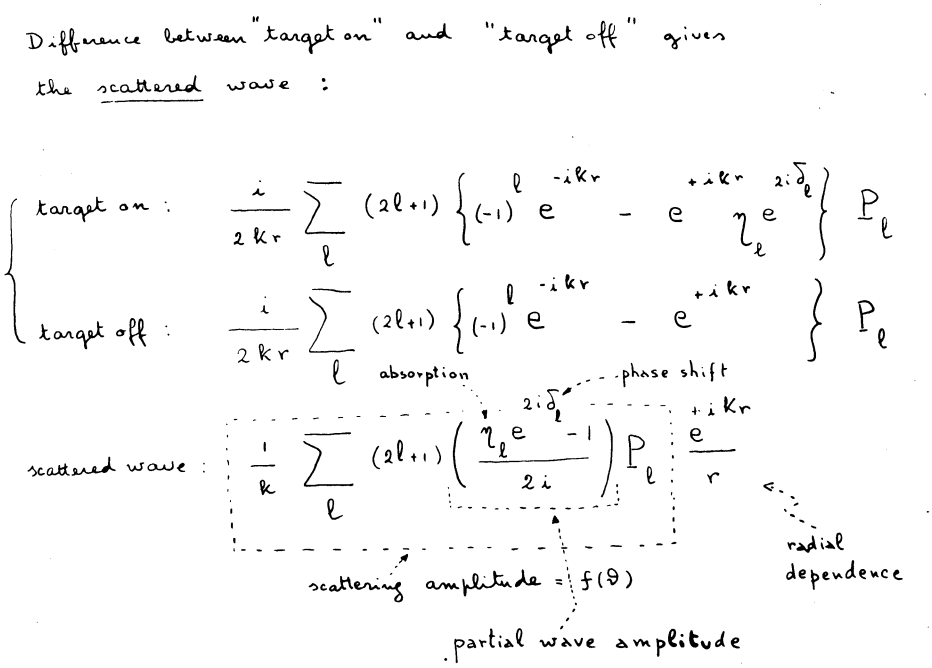

Fig. 14

Thus, according to its energy dependence, the ℓ^{th} partial wave will be labelled as "resonant" or as "background" or as a mixture of the two. It is then important to examine in some more detail how the partial waves are related to the observable quantities. What can be measured, in practice, is the flux of scattered particles in a certain direction, normalized to the flux of incident particles; this is what is called "scattering"cross section. Fig. 15(a) shows the connection between the partial waves and the "scattering" or "elastic" cross section in the differential and integrated form. When the final state particles are not the same as in the initial state, then the partial waves describing the phenomenon are those referring to the "absorption" or "reaction" processes. In a manner analogous to that of Fig. 15(a) one can show that the flux of the absorbed part of the incident wave, again normalized to the incident flux, is related to the "absorption" or "reaction" cross section through the expression of fig. 15(b). Due to the unitarity requirements, the two cross sections, elastic and reaction, must be related to one another. The connection, as can be seen in fig. 15, is through the absorption parameter η. Unitarity requires that η^2 should not exceed 1. Notice that the

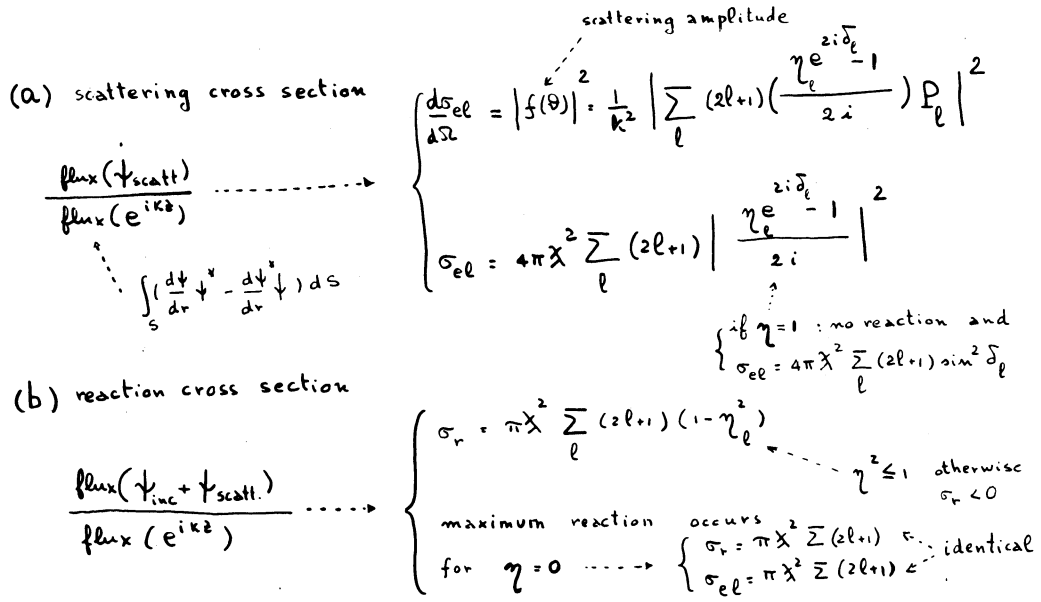

Fig. 15

reaction cross section should be understood as the sum over all possible reaction channels; one can, of course, subdivide η into as many absorption parameters, η_i, as there are reaction channels, with the unitarity condition becoming then $\sum_i \eta_i^2 \leq 1$. The relation between σ_{el} and σ_r is given graphically in fig. 16 for different values of the phase shift δ. From the above results and the scattering amplitude in fig. 14 one can easily put together the so-called "optical theorem" (fig. 17). The latter is quite useful because it connects our unknown partial wave amplitudes to an easily measurable quantity, the total cross section.

The next three figures, from 18 to 20, provide the extension to the case of a spin 0 particle incident on a spin 1/2 target. This is our practical case of interest, applying to πN and KN scattering. A straightforward extension, valid for the integrated cross sections is shown in fig.18 and consists in replacing the statistical factor $2\ell + 1$ with $J + 1/2$ and introducing for each value of ℓ a partial wave amplitude T_ℓ^+ corresponding to $J = \ell + 1/2$ and another T_ℓ^- corresponding to $J = \ell - 1/2$. The extension of the differential cross section to this case is not straightforward and

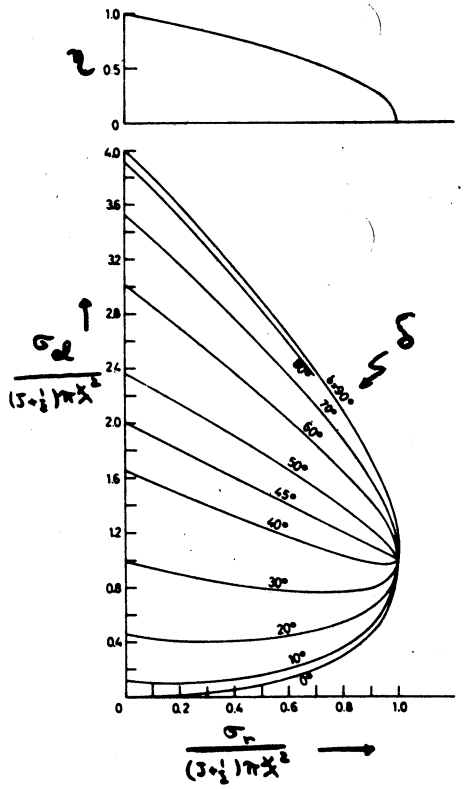

Fig. 16

OPTICAL THEOREM

$$\begin{cases} \sigma_{el} = 4\pi\lambda^2 \sum_l (2l+1) \left| \dfrac{\eta_l e^{2i\delta_l} - 1}{2i} \right|^2 \\ \sigma_r = \pi\lambda^2 \sum_l (2l+1)(1-\eta_l^2) \end{cases}$$

$$\sigma_{el} + \sigma_r = 2\pi\lambda^2 \sum_l (2l+1)(1-\eta_l \cos 2\delta_l)$$

scattering amplitude $[d\sigma/d\Omega = |f(\theta)|^2]$

$$\begin{cases} f(\theta) = \dfrac{1}{k} \sum_l (2l+1) \left(\dfrac{\eta_l e^{2i\delta_l} - 1}{2i} \right) P_l(\cos\theta) \\ f(\theta=0) = \dfrac{1}{k} \sum_l (2l+1) \left(\eta_l \dfrac{e^{2i\delta_l} - 1}{2i} \right) \end{cases}$$

$$\mathrm{Im}\, f(0) = \frac{1}{2k} \sum_l (2l+1)(1-\eta_l \cos 2\delta_l)$$

forward scattering amplitude

$P_l(\cos\theta = 1) = 1$

$$\boxed{\sigma_{tot} = \frac{4\pi}{k} \mathrm{Im}\, f(0)}$$

i.e. "optical theorem".

partial wave amplitudes

equivalent to : $\sigma_{tot} = 4\pi\lambda^2 \sum_l (2l+1) \mathrm{Im}\, T_l$

substitute with $J+\frac{1}{2}$ and $T_l^{\pm}$ when target has spin $\frac{1}{2}$.

Fig. 17

TARGET WITH SPIN $\frac{1}{2}$:

a) $2\ell+1$ (statistical factor) ------▶ $\dfrac{2J+1}{(2S_1+1)(2S_2+1)}$ ------▶ $J+\frac{1}{2}$ for $\begin{cases} S_1=\frac{1}{2} \\ S_2=0 \end{cases}$

($2J+1$: total spin (target + incid.); $2S_1+1$: target spin ($S_1=\frac{1}{2}$); $2S_2+1$: incident spin ($S_2=0$))

b) $\eta_\ell e^{2i\delta_\ell}$ -----▶ $\begin{cases} \eta_\ell^+ e^{2i\delta_\ell^+} & \text{(spin up)} \quad J=\ell+\frac{1}{2} \\ \eta_\ell^- e^{2i\delta_\ell^-} & \text{(spin down)} \quad J=\ell-\frac{1}{2} \end{cases}$

c) $\begin{cases} \sigma_{el} \text{ ---▶ } 4\pi\lambda^2 \sum (J+\frac{1}{2}) |T_\ell^\pm|^2 \\ \sigma_r \text{ ---▶ } \pi\lambda^2 \sum (J+\frac{1}{2}) (1-\eta_\ell^{\pm 2}) \end{cases}$ ------ partial wave ampl. for orbital ang. mom. ℓ and spin up (+) or down (-) ------▶ $T_\ell^\pm = \dfrac{\eta_\ell^\pm e^{2i\delta_\ell^\pm} - 1}{2i}$

EXTENSION TO $\frac{d\sigma}{d\Omega}$ IS <u>NOT</u> SO SIMPLE (SEE NEXT FIGURE)

Fig. 18

SCATTERING OF SPIN 0 ON SPIN $\frac{1}{2}$

(for example, πN and KN scattering)

$$\frac{d\sigma}{d\Omega} = (\psi_f^\dagger, \psi_f) = \frac{1}{2} \mathrm{Tr}(M^\dagger M) = |f|^2 + |g|^2$$

($|f|^2$: non-spin-flip amplitude; $|g|^2$: spin-flip amplitude; ψ_f: final state wave function)

$$\psi_f = M \chi_i$$

(χ_i: initial spin state; M: transition matrix)

$$M = f(\theta) + g(\theta)\, \vec{\sigma}\cdot\vec{n}$$

($f(\theta)$: operates on the spin state as it is; $\vec{\sigma}\cdot\vec{n}$: flips the spin state; operates on the flipped spin state; $\vec{\sigma}$ = Pauli spin operator; $\vec{n} = \vec{k}_i \times \vec{k}_f$)

$$\frac{d\sigma}{d\Omega}\vec{P} = (\psi_f^\dagger, \vec{\sigma}\psi_f) = \frac{1}{2}\mathrm{Tr}(M^\dagger \vec{\sigma} M) = 2\,\mathrm{Re}(f^* g)\,\vec{n}$$

($\vec{P}$: polarization of the final state spin $\frac{1}{2}$ particle)

Fig. 19

EXPANSION OF THE NON-SPIN-FLIP (f) AND THE SPIN-FLIP (g) AMPLITUDE IN TERMS OF PARTIAL WAVES ($T_\ell^\pm$)

$$\begin{cases} f(\vartheta) = \frac{1}{k} \sum_\ell \left[(\ell+1) T_\ell^+ + \ell\, T_\ell^- \right] P_\ell(\cos\vartheta) \\ g(\vartheta) = \frac{i}{k} \sum_\ell \left[T_\ell^+ - T_\ell^- \right] P_\ell^1(\cos\vartheta) \end{cases}$$

P_ℓ^1 : first associated Legendre polynomial

$$\begin{cases} \frac{d\sigma}{d\Omega} = |f(\vartheta)|^2 + |g(\vartheta)|^2 \\ \vec{P}\frac{d\sigma}{d\Omega} = 2\,\mathrm{Re}(f^* g)\,\vec{n} \end{cases}$$

example : only $\ell=0$ and $\ell=1$ partial waves :

$$\frac{d\sigma}{d\Omega} = \frac{1}{k^2}\left| T_0^+ P_0 + (2T_1^+ + T_1^-) P_1 \right|^2 + \frac{1}{k^2}\left| (T_1^+ - T_1^-) P_1^1 \right|^2$$

$$\sigma = \int \frac{d\sigma}{d\Omega} d\Omega = \frac{4\pi}{k^2}\left\{ |T_0^+|^2 + |2T_1^+ + T_1^-|^2 \tfrac{1}{3} + |T_1^+ - T_1^-|^2 \tfrac{2}{3} \right\} =$$

$$= \frac{4\pi}{k^2}\left\{ |T_0^+|^2 + |T_1^-|^2 + 2|T_1^+|^2 \right\}$$

notation : $S_{1/2}$ $P_{1/2}$ $P_{3/2}$

i.e. equivalent to $\sigma = 4\pi\lambda^2 \sum (J+\tfrac{1}{2}) |T_\ell^\pm|^2$

Fig. 20

FUNDAMENTAL AMBIGUITIES IN THE DETERMINATION OF THE PARTIAL WAVES ($T_\ell^\pm$).

(a) MINAMI AMBIG. : $\vec{\sigma}\cdot\vec{k}$ = scalar operator, odd under parity (inverts parity)

leaves J invariant

$M' = \vec{\sigma}\cdot\vec{k}_f \; M \; \vec{\sigma}\cdot\vec{k}_i$

leaves J but inverts init. and final parities

result → $\begin{cases} \frac{d\sigma}{d\Omega} \text{ remains identical} & (I' = I) \\ \text{polarization changes sign} & (P' = -P) \end{cases}$

example : $S_{1/2} \rightleftarrows P_{1/2}$ $\quad P_{3/2} \rightleftarrows D_{3/2}$ $\quad D_{5/2} \rightleftarrows F_{5/2}$ ... and all the others ...

(b) COMPLEX CONJUGATION AMBIG. :

$T \to T^*$ result → $\begin{cases} I' = I \\ P' = -P \end{cases}$ because $I\vec{P} = 2\,\mathrm{Re}(f^* g)\,\vec{n}$

$f = F(T_\ell^\pm)$; $g = i\,G(T_\ell^\pm)$

Fig. 21

requires the steps indicated very briefly in fig. 19. A new quantity directly measurable is also introduced in this case; the polarization $\vec{P}$. Absent in the spinless case (see fig. 20: $T_\ell^+ = T_\ell^-$ gives $g(\vartheta) = 0$, thus $\vec{P} = 0$), the polarization becomes an additional piece of information when dealing with πN and $\bar{K}N$ scattering.

We have now in our hands all the practically useful relations connecting partial waves ($T_\ell^{\pm}$) and measurable quantities ($d\sigma/d\Omega$, $\vec{P}$). Even before writing down explicitly the expression, one can already see that, no matter how skillful one is when solving the problem, the above formulae present certain properties which impede a complete solution. Referring to fig. 21, one can see that, under what is called a "Minami transformation", the differential cross section remains unchanged and the polarization changes sign. But this is also what happens under a "complex-conjugation transformation, so that the combined application of (a) and (b) leaves all our measured quantities as they are, while turning the amplitudes into the complex conjugate of their Minami transform. This is more embarrassing than it may look at first sight, because it is equivalent to saying that the <u>parity</u> of all our partial waves is undefined, thus depriving us of what seemed like a very good tool for finding out the spin and parity of the resonances. Fortunately there is something else that comes to help here. Let us suppose that the energy available in the centre of mass is just above threshold for the reaction to occur (it may be elastic scattering or an absorption process); then the above embarrassment of choice between, say, $\ell = 0$ and $\ell = 1$ is much less severe because all possible dynamical considerations point to the lower value of ℓ. Thus we may feel reasonably sure that S-waves predominate near threshold (and this, for example, has been verified in all the detailed studies of low energy $\bar{K}N$ and πN interactions). It goes by itself that, once <u>one</u> amplitude is identified, then it suffices to follow that amplitude throughout its energy variation in order to have always a fixed reference point for the other amplitudes. In this connection, fig. 22 shows a possible behaviour expected for the partial waves near threshold; this is the "effective-range expansion", based on dynamical assumptions and valid only

at low energies. An amplitude, for example, which follows the prescriptions of fig. 22(b) will have a different energy dependence according to its ℓ-value and, although at a certain moment the effective range approximation

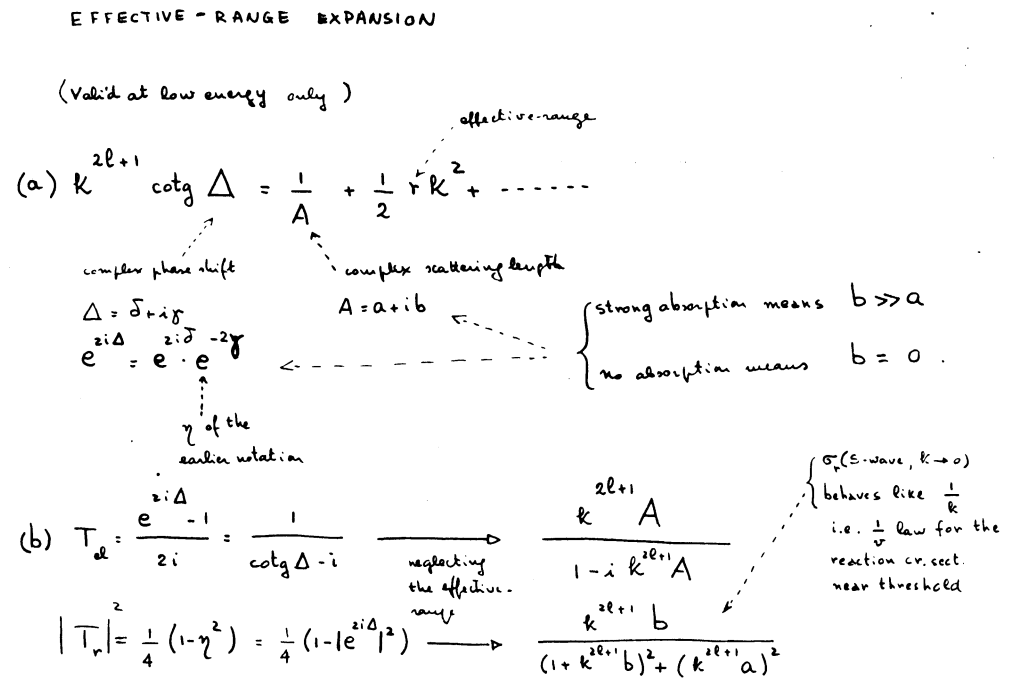

Fig. 22

will no more be valid, the knowledge of this amplitude in its early development provides a natural basis for its continuation at higher energies. One should not neglect the possibility, on the other hand, that different threshold behaviours are also possible. The example in fig. 23 shows that, at least for the $K^- p \to \Lambda \eta$ reaction near threshold, a resonant S-wave behaviour fits the data better than the S-wave predictions of a zero-effective-range expansion. A P-wave behaviour is not excluded either; however, the complete absence of S-waves (as required by the differential cross sections which are isotropic in the whole energy region, thus excluding S-P interference)is not a very likely situation. Thus the preference to a resonant S-wave when explaining the data[14].

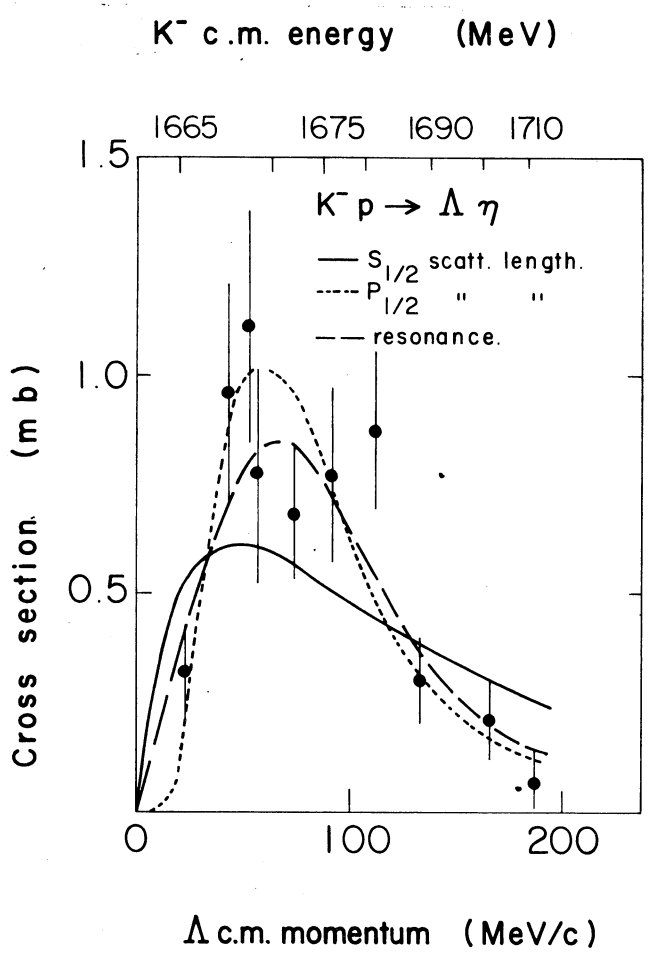

Fig. 23

BREIT-WIGNER FORMULA

(valid near resonance)

(a) $\cot g\,\delta = \frac{1}{kA} + \cdots\cdots$ shows that $\cot g\,\delta$ is a function of E.

($\frac{1}{kA}$: case of S-wave elastic scattering)

$$\cot g\,\delta = 0 + (E_R - E)\left[\frac{d\cot g\,\delta}{dE}\right]_{E_R} + \cdots\cdots = (E_R - E)\frac{2}{\Gamma} + \cdots\cdots$$

(define this deriv. as $\frac{2}{\Gamma}$; 0: expansion around E_R, where $\delta = \frac{\pi}{2}$)

$$T_{el} = \frac{1}{\cot g\,\delta - i} \longrightarrow \frac{1}{(E_R - E)\frac{2}{\Gamma} - i} = \frac{1}{\varepsilon - i}$$

($(E_R - E)\frac{2}{\Gamma}$: call this ε)

$$|T_{el}|^2 = \frac{\Gamma^2}{(E_R - E)^2 + \frac{\Gamma^2}{4}}$$

(Γ: full width of res.)

(b) $\psi(t) = e^{-\frac{t}{2\tau}} e^{-i\frac{E_R}{\hbar}t}$ $\longrightarrow$ $\Phi(E) = \int_0^\infty \psi(t)\, e^{i\frac{E}{\hbar}t} = \frac{1}{(E_R - E) - i\frac{\hbar}{2\tau}}$

($\psi(t)$: state with mean-life τ; $\Phi(E)$: Fourier transform of ψ)

$\Gamma = \frac{\hbar}{\tau}$ from the uncertainty principle

Fig. 24

IV. Breit-Wigner resonance formula

This brings up the last item of this lecture: the behaviour of resonant partial waves. The term, as applied until now, was used rather loosely and it is now time to see what we mean. In fig. 24 two examples are outlined of how the Breit-Wigner resonance formula can be simply derived[4]. The formula arrived at, although not relativistic, is good enough for most present-day applications. In any case, it should not be extended too far from resonance (no more than a couple of widths, say). The energy dependence of the width itself introduces another source of controversy; we shall come back to this point later. For the moment let us neglect the energy dependence and assume Γ constant. Under the above assumptions, it is easy to visualize the energy behaviour of a Breit-Wigner resonant amplitude. Fig. 25 shows how this amplitude describes a circle in the complex plane and how the size of the circle is related to the "elastic" or "reaction" branching fraction of the resonance. The relation is more apparent in

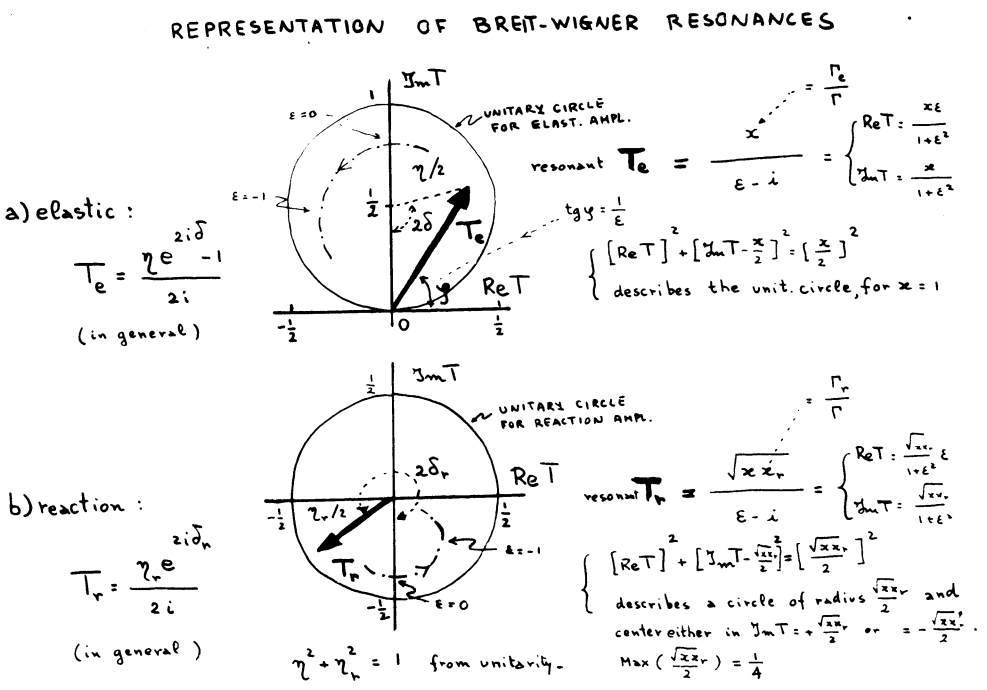

Fig. 25

fig. 26, where three typical cases are given for the elastic channel: $x = 1$ (maximum elasticity), $x = 1/2$ (maximum reaction), $x = 1/4$ (small elasticity, small reaction). The corresponding circles shrink progressively (from the maximum, called "unitary circle", with unit diameter, to one having

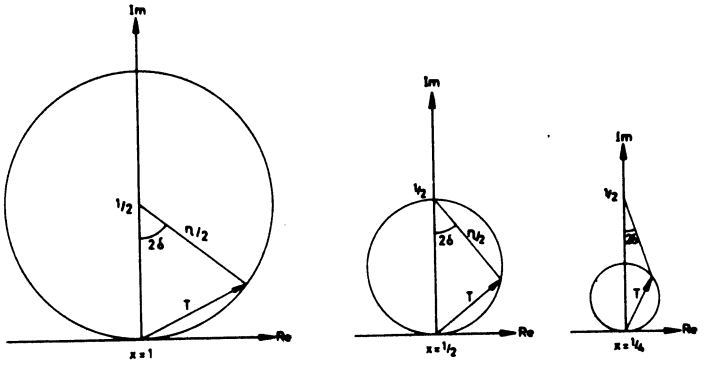

Fig. 26

a diameter of 1/4). At is interesting to notice that, while the resonant amplitude will always go along a circle, the behaviour of the phase shift δ and absorption parameter η as a function of energy (fig. 27) is instead very different according to the different cases. Although the information contained by the two representations is clearly the same, the above example speaks much in favour of the complex plane representation when studying the behaviour of an unknown amplitude.

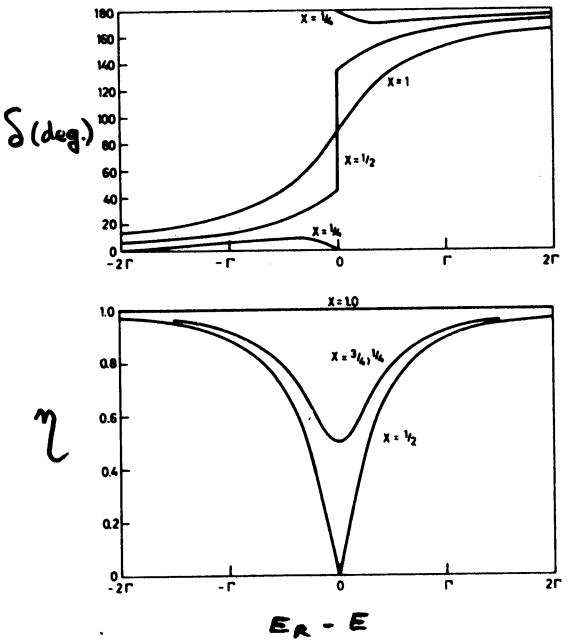

Fig. 27.

As was already pointed out at the beginning (figs. 7 to 9), the most obvious manifestation of a resonant amplitude can usually be found in the shape of its cross section. Fig. 28 shows what to expect from the latter on the basis of the previous formulae. Elastic, reaction and total cross

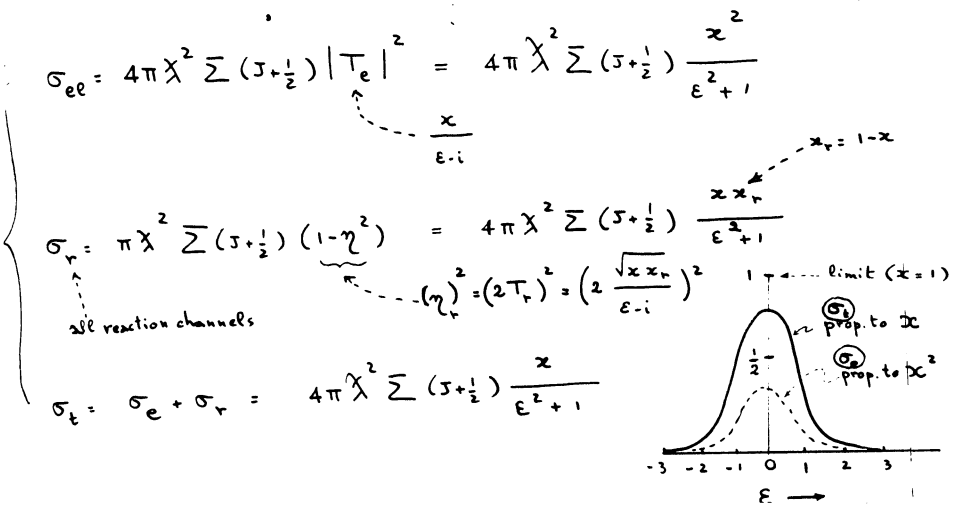

Fig. 28

sections all vary with energy in the same manner, the size of their respective enhancements being in the ratio of $x^2 : x(1-x) : x$. Since x is always smaller than 1, a notable consequence is that looking for resonant enhancements in the elastic cross section is in principle more difficult than in the total cross section. However, there are other considerations - like the size and shape of the background - which must be taken into account before agreeing with the above simple conlusion.

Finally, one word about the energy dependence of the width. Fig. 29 shows the two main approaches to this problem. It should be stressed that, in most practical cases, the difference between the two is well beyond the experimental accuracy; furthermore neither case is appropriate enough when too far away from the resonance.

ENERGY DEPENDENCE OF PARTIAL WIDTHS

$$\Gamma \propto \left(\frac{k}{E}\right) \times B_\ell(k)$$

phase space

centrifugal barrier →

- k : final state wave number
- E : total energy

(a) relativistic parametrization :

$$B_\ell = \left(\frac{k^2}{k^2 + X^2}\right)^\ell , \quad X \sim 350\,\text{MeV}$$

(b) non-relativistic expression (square-well potential) : $B_0 = 1$

$r \sim 1$ fermi

$$B_1 = \frac{(kr)^2}{1+(kr)^2}$$

$$B_2 = \frac{(kr)^4}{9+3(kr)^2+(kr)^4}$$

etc. . . . . .
(small ℓ)

Fig. 29

- o -

SECOND LECTURE

V. Partial wave analysis of the $\bar{K}N$ system

We can now go back to our subject, i.e. hyperon resonances and how to study them. The most accessible experiment in order to "form" hyperon resonances is to scatter K^- mesons on protons. This has been done with both counters and bubble chambers, up to energies of $\sim$ 3 GeV/c, i.e. masses of the $\bar{K}N$ system of 2.6 GeV. The two techniques are complementary: the total and elastic cross section (with or without a polarized target) being measured better and more easily with counters, the other channels being fully exploited only with bubble chambers.

Fig. 30 shows an early collection (circa 1962) of total cross section data[15] resulting from various experiments. Quite outstanding is a pronounced enhancement near 1800 MeV, ascribed then to the formation of a

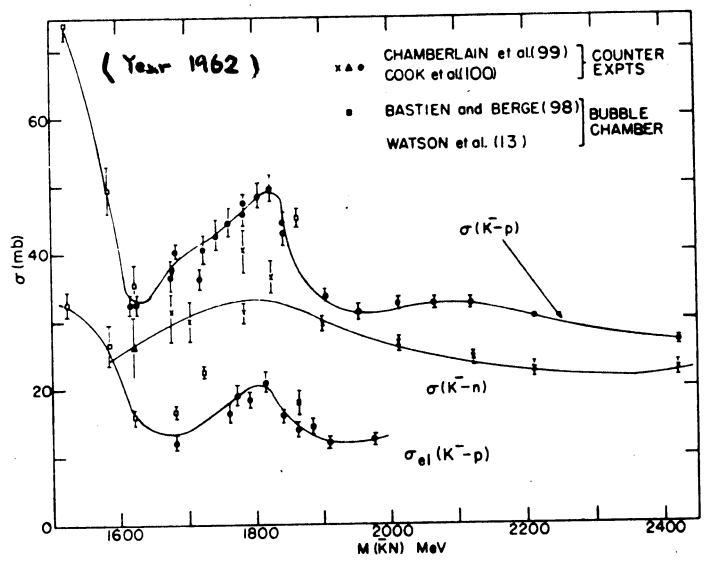

Fig. 30

resonance, $\Lambda(1820)$. We have already seen in fig. 9 how much better known this momentum region is nowadays and how many more resonances have come up when the same measurements were repeated with better accuracy and statistics. We

shall see now that even the situation represented in fig. 9 is still inadequate for a full understanding of the phenomena taking place in this region. In order to do so, we shall examine in detail the procedure and results of a partial wave analysis of the $\bar{K}N$ system in the region of the above enhancement[1] Fig. 31 shows what reactions one has to deal with in this energy region. Notice that the analysis in the form described below

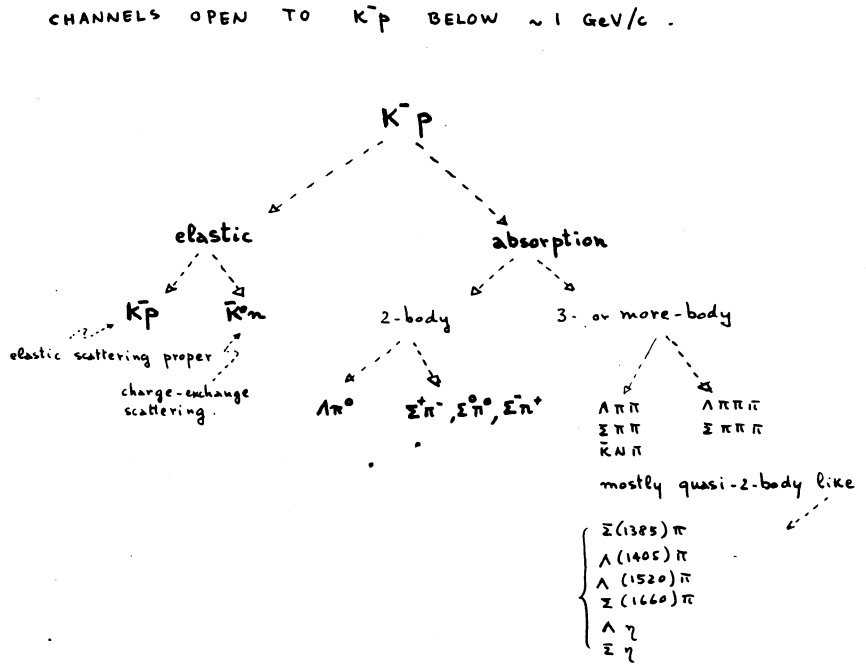

Fig. 31

has only been performed on the 2-body processes, the remaining reactions being either too scarce for a meaningful interpretation or too complicated for this simplified approach. To have an idea of the behaviour of the data in our and other momentum regions, let us examine figs. 32 and 33. They give the momentum dependence of the ratio between cross section σ and $4\pi\lambda^2$ (the "geometrical" factor in the formulae of fig. 18) for the two elastic channels. The arrows indicate the position of the better established resonances (as identified by this and other experiments[16]), the full circles refer to the data of this experiment. It is interesting to notice how fundamentally different is the "background" behaviour of these two

channels. In the $\bar{K}^0 n$ case the resonances are superposed to an almost constant and small background, they are clearly distinguishable and a more accurate study of this cross section may well uncover some yet unknown structure. The background for the $K^- p$ case is, instead, of a quite different nature: it is large and appears to be growing steadily with increasing momentum. This is clearly not the best channel to look into when hunting for small resonant structures.

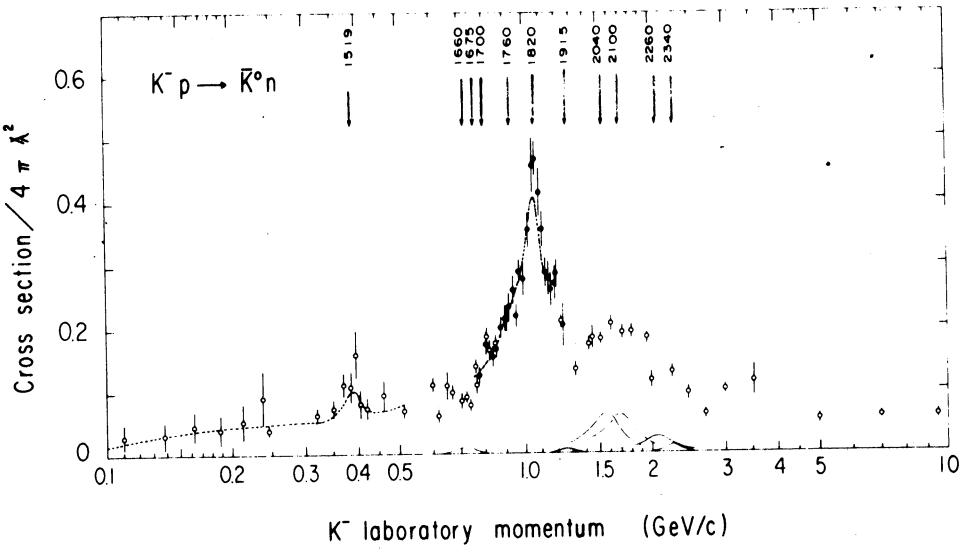

Fig. 32

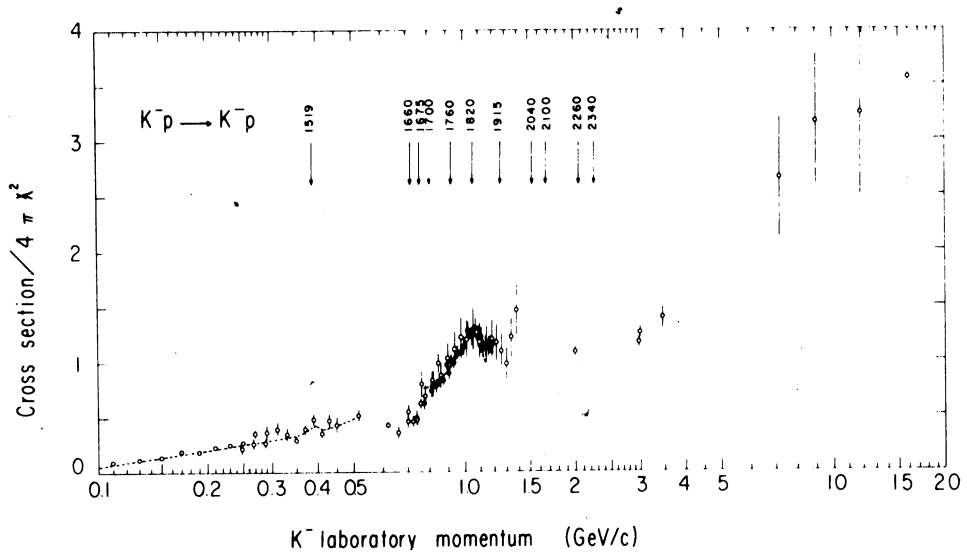

Fig. 33

Turning now to the partial waves, the starting point is the expression of $d\sigma/d\Omega$ in fig. 20. Writing it explicitly in terms of partial waves gives the formula of Fig. 34. It is possible and convenient to expand this formula in a series of Legendre polynomials; the coefficients of the

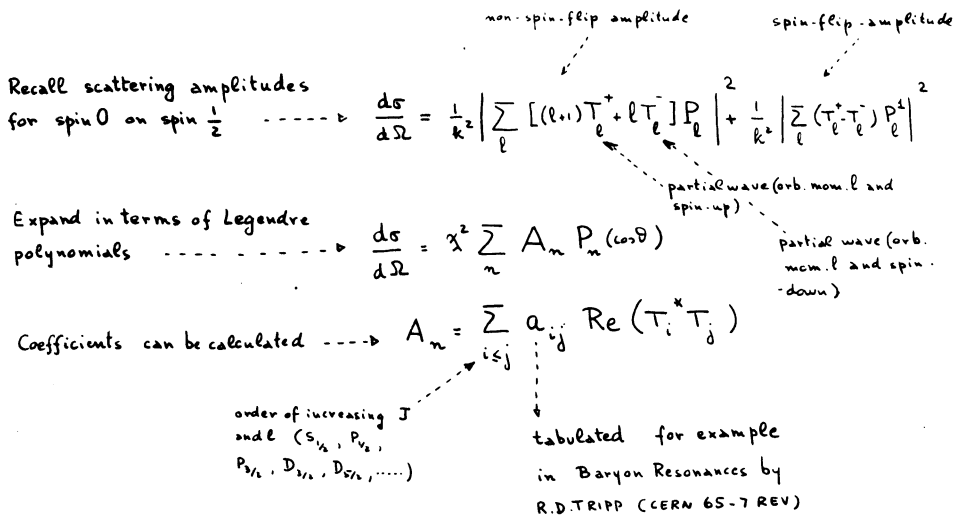

Fig. 34

expansion can be calculated and tabulations exist[4] connecting them with the partial wave amplitudes $T_\ell^{\pm}$. The same operation can be performed on $\vec{P}(d\sigma/d\Omega)$ (fig. 35), except that here the most convenient expansion is one

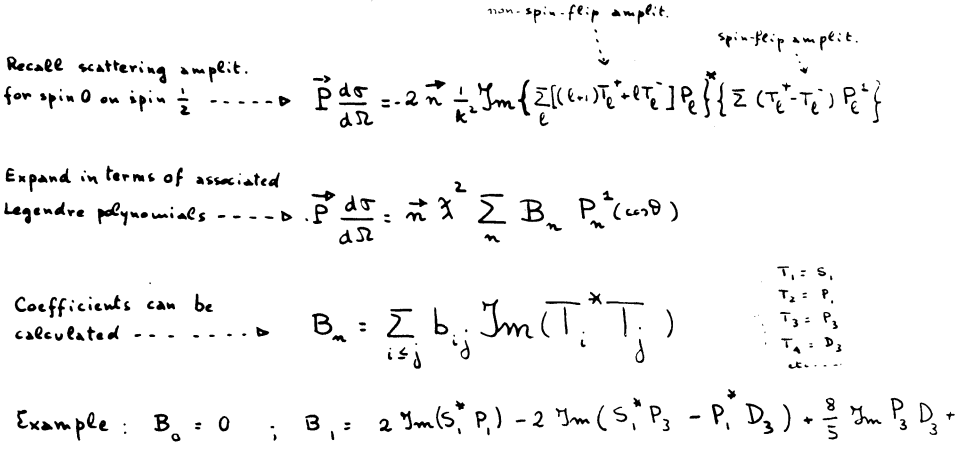

Fig. 35

in terms of associated Legendre polynomial of the first order. Here also the coefficients of the expansion can be calculated or read out from existing tabulations. Exactly the same expansions can be performed on the experimental differential cross sections (fig. 36) and we finally end up with <u>experimental</u> coefficients A_n and B_n to be compared with the expressions

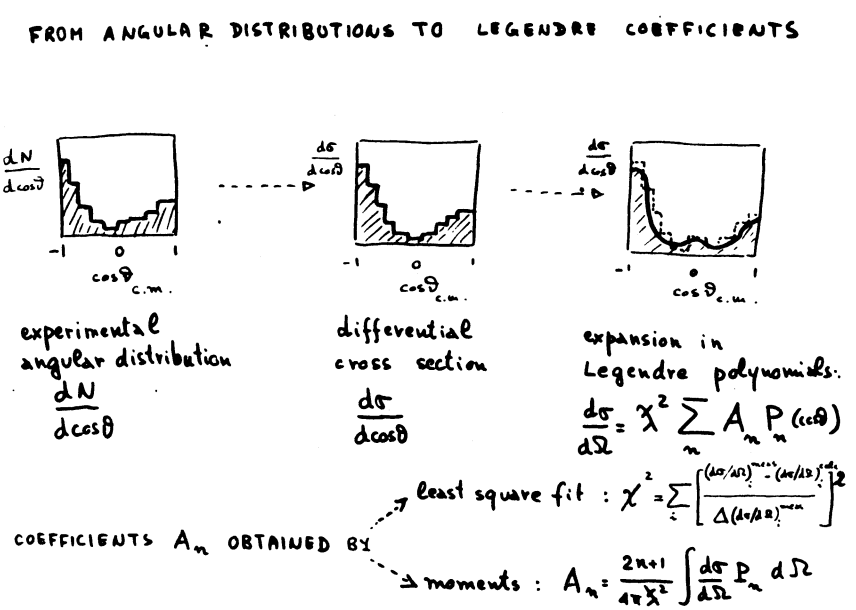

Fig. 36.

involving the desired partial waves (see some examples of these in figs. 34 and 35). Fig. 37 shows how some of the angular distributions look and fig. 38 gives the experimental coefficients of their Legendre polynomial expansion as a function of the incident K^- momentum. These coefficients (and those of the other reactions) are the <u>data</u> and from them we shall try to extricate the partial waves. It should be mentioned that the procedure of going through the Legendre coefficients is by no means universal; the connection with the partial waves can be made directly through the differential cross sections, comparing the experimental values of $d\sigma/d\Omega$, subdivided in convenient intervals of $\cos\vartheta$, with the corresponding expressions of fig. 34 and 35 with P_n and P_n^1 evaluated at the central value of $\cos\vartheta$ for the interval in question. The advantage of using the Legendre

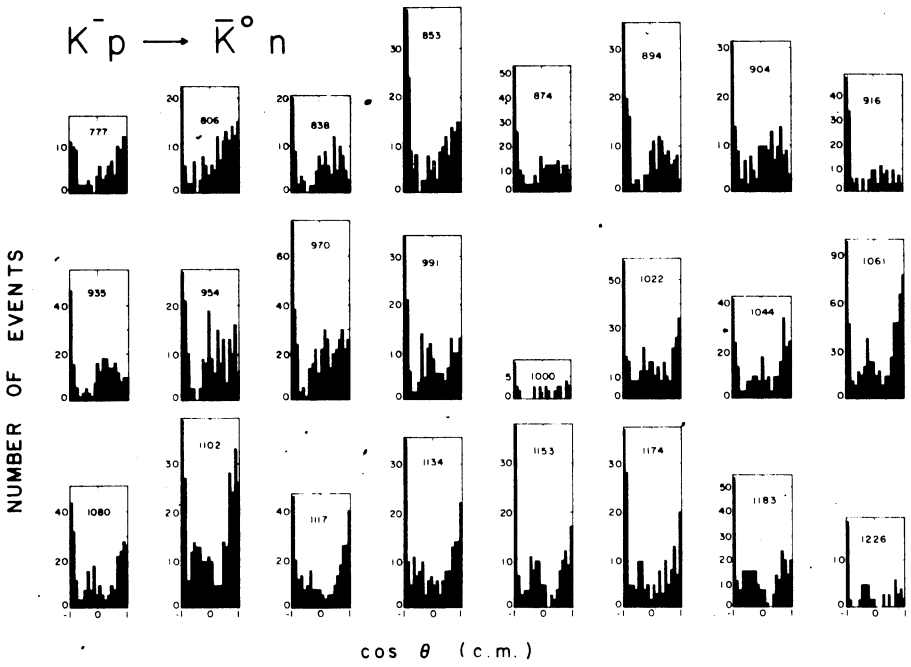
K⁻p ⟶ K̄°n
NUMBER OF EVENTS
cos θ (c.m.)

Fig. 37

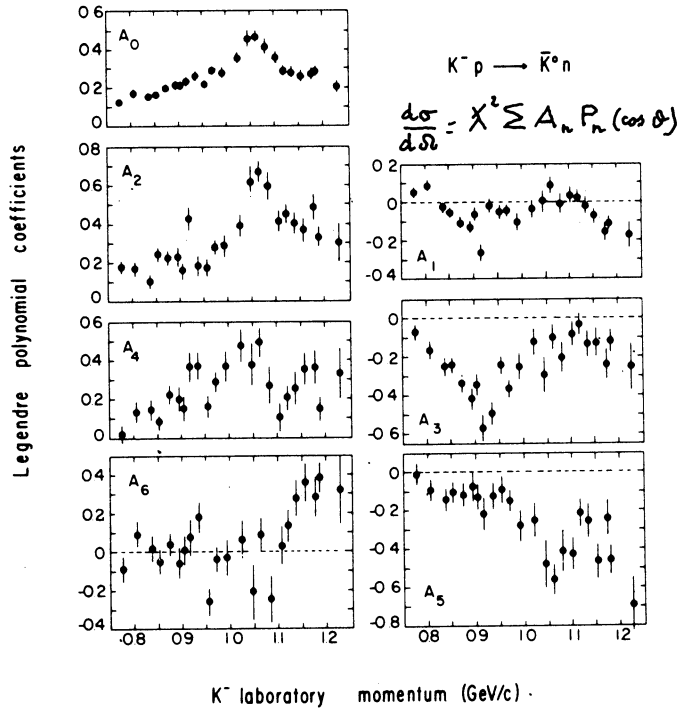
K⁻p ⟶ K̄°n
dσ/dΩ = λ² Σ Aₙ Pₙ (cos θ)
Legendre polynomial coefficients
K⁻ laboratory momentum (GeV/c)

Fig. 38

coefficients, although criticizable as statistically less sound, lies mainly in the intuitive appreciation they allow for the behaviour of the partial waves, appreciation which is totally lost in the other approach. Thus the behaviour of a certain coefficient as a function of energy can be easily related to the nature of the partial waves contributing to it.

As an example, let us consider the data of fig. 38. The conspicuous enhancement of A_o near 1 GeV/c tells us that something must be resonant in this neighbourhood. On the other hand, any of the partial waves could be responsible for the enhancement ($A_o = S^2 + P_1^2 + 2(P_3^2 + D_3^2) + 3(D_5^2 + F_5^2) + ...$). But A_6, together with the higher coefficients, is consistent with zero, thus implying that waves with $J > 5/2$ are absent or at least negligible in this region. A_5 is instead different from zero; with the maximum value of J being limited to 5/2, the expression of A_5 as a function of the partial waves is particularly simple: $A_5 = \frac{100}{7} \text{Re}\,(D_5^* \cdot F_5)$. Thus the fact that A_5 shows a sudden and large negative excursion conveys that either D_5 or F_5 must be both present and at least one of them quickly varying. Remembering now the properties of a resonant amplitude in the elastic channel as illustrated in fig. 25, one can explain the enhancements in A_o and A_5 as for position, magnitude and shape by simply assuming that both D_5 and F_5 are resonant at about the same energy. The above qualitative argument is further stengthened by the behaviour of the other elastic channel, $K^-p \to K^-p$ (a different combination of the same isotopic spin amplitudes; see fig. 40 below). In this way one can also show that the resonant D_5 and F_5 amplitudes must be in different states of isotopic spin (the excursion of A_5 in $K^-p \to K^-p$ having opposite sign than that in $K^-p \to \bar{K}^o n$). There are considerations of background which have been left out of this simplified discussion and we also have neglected the information coming from the other coefficients. Still the above conclusions[17] are valid and borne out by the quantitative analysis discussed below. It goes by itself that the same type of considerations are much more difficult, if not impossible, when staring at the differential cross sections themselves (fig. 37). There, rather, one may well be tempted into invoking phenomena such as "baryon exchange" (look at all those backward peaks ...) or some other unnecessarily

involved mechanism which may not offer as simple and as consistent a picture as that in terms of resonant partial waves in the direct channel.

Proceeding with the partial wave analysis, fig. 39 shows what one knows or suspects (from previous experiments, qualitative considerations of the type indicated above, personal prejudices etc...) about the amplitudes

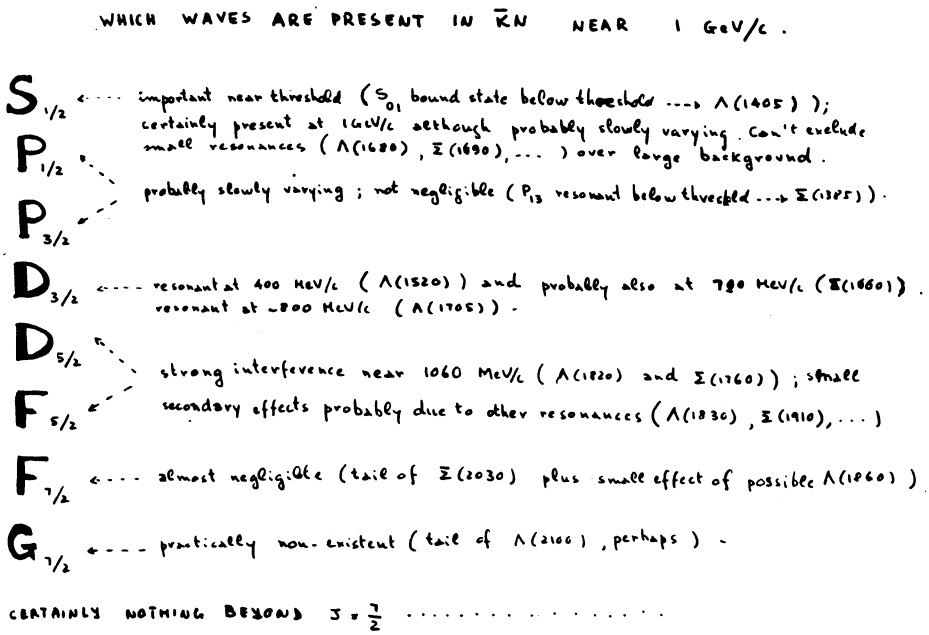

Fig. 39.

present near 1 GeV/c. This list needs further to be enlarged in order to make space for the two possible isotopic spin states of the $\bar{K}p$ system. The isotopic spin composition of the channels considered in the analysis is given in fig. 40 together with a quick reminder of how it was obtained. We are now ready to investigate the energy dependence of each amplitude; from now on, the assumptions, simplifications and procedures are all specific to the problem in question and refer only to the particular approach adopted in ref. 1.

As it will be more clear later on, there isn't enough experimental

information to solve the problem at each momentum. One is instead obliged to

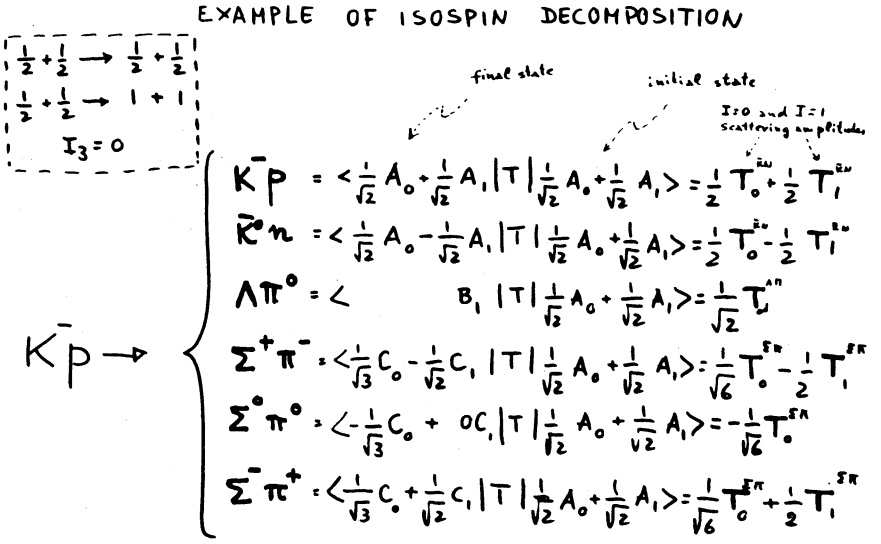

Fig. 40.

assume a certain momentum dependence of the amplitudes and then try to solve over many momenta at the same time. Three explicit parametrizations are shown in fig. 41, together with the number of unknowns required by each one of them. The parametrization indicated as (c) has not really been used; it is mentioned here only as a warning against such a simple minded approach.

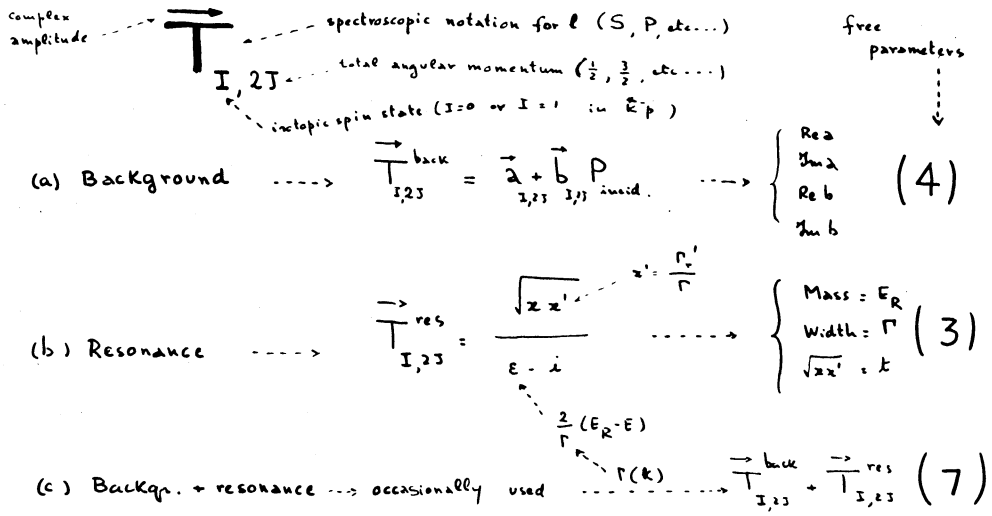

Fig. 41.

The correct way of adding up a background and a resonance with the same quantum numbers is more complicated, as can be seen for example in fig. 42 which shows the elastic case only[15]. The parametrizations of fig. 41 are now imposed on the waves of fig. 39 according to the known or suspected character of these waves. Different combinations of resonant and background are then tried until a satisfactory solution is eventually reached and one is reasonably sure that alternative possibilities do not exist. How this is done in practice can be followed through figs. 43 and 44. First, our 16 waves are parametrized as (for example) in the manner listed at the left of fig. 43. In the same figure one can also see how many data are available for each channel and at each momentum. It immediately appears that only in the case of the $A\pi$ reaction is there an equal number of data and unknowns (an overall undetermined phase brings down the 16 $A\pi$ unknowns to 15). Thus our system of equations (each data point is an equation) is largely underconstrained; a solution momentum by momentum is clearly impossible. The situation instead looks different when we count the free variables of our parametrization: already 3 different momenta are sufficient in order to have more equations than unknowns. The momenta available in the experiment are about 20, spread out over some 400 MeV/c (corresponding to ~ 200 MeV in centre of mass energy). The system is thus well overconstrained and the existence of a solution depends only on the validity of the hypotheses and the reliability of the data. It is also clear that such a large amount of computation cannot be carried on by hand; the flow diagram in fig. 44 shows the main steps followed in a computer search for the best solution. The method used is that of finding the parameters corresponding to a minimum of χ^2; one could, alternatively, use a maximum-likelihood

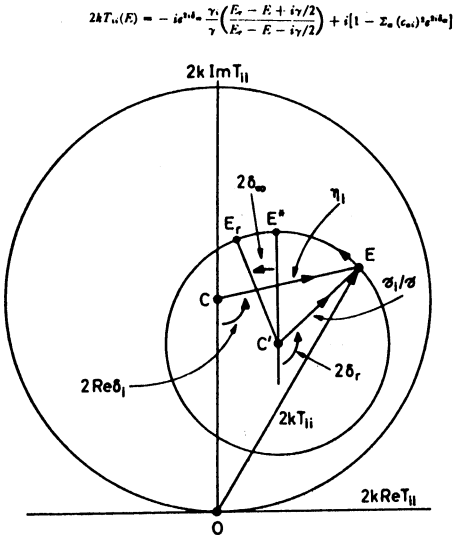

Fig. 42.

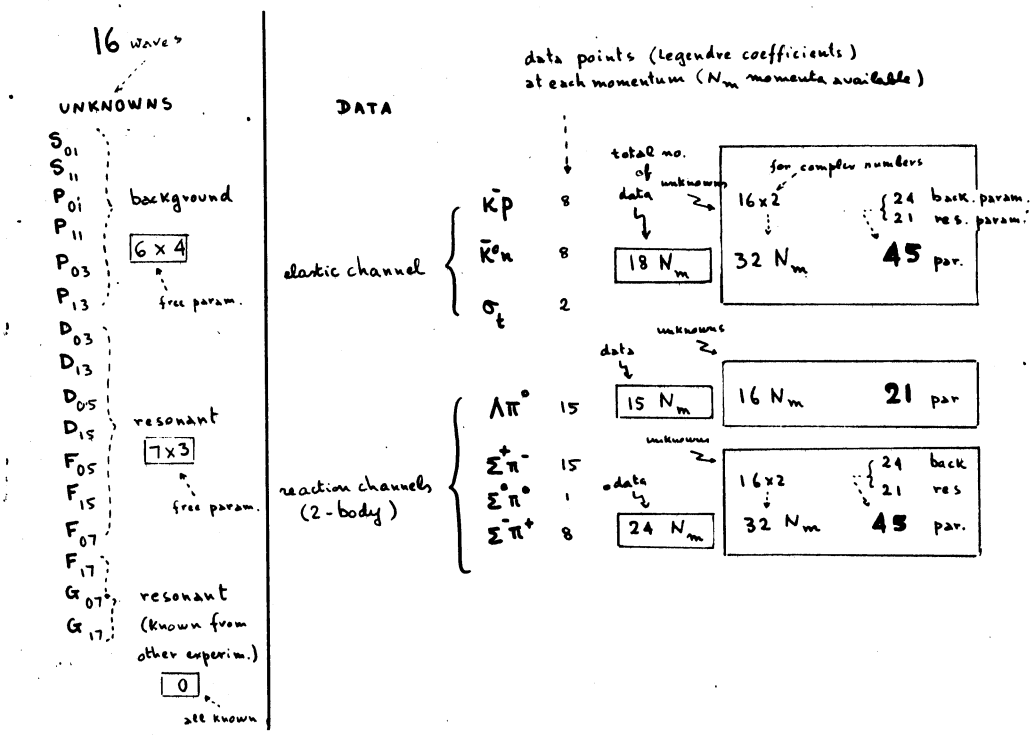
16 waves
UNKNOWNS
S_{01}
S_{11}
P_{01}
P_{11}
P_{03}
P_{13}
background
6 x 4
free param.
D_{03}
D_{13}
D_{05}
D_{15}
F_{05}
F_{15}
F_{07}
resonant
7x3
free param.
F_{17}
G_{07}
G_{17}
resonant
(known from other experim.)
0
all known
DATA
data points (legendre coefficients)
at each momentum (N_m momenta available)
total no. of unknowns
for complex numbers
elastic channel
$\bar{K}p$ 8
$\bar{K}^0n$ 8
σ_t 2
data
18 N_m
16x2
32 N_m
24 back. param.
21 res. param.
45 par.
unknowns
data
15 N_m
16 N_m
21 par
reaction channels (2-body)
$\Lambda\pi^0$ 15
$\Sigma^+\pi^-$ 15
$\Sigma^0\pi^0$ 1
$\Sigma^-\pi^+$ 8
unknowns
data
24 N_m
16x2
32 N_m
24 back
21 res
45 par.

Fig. 43

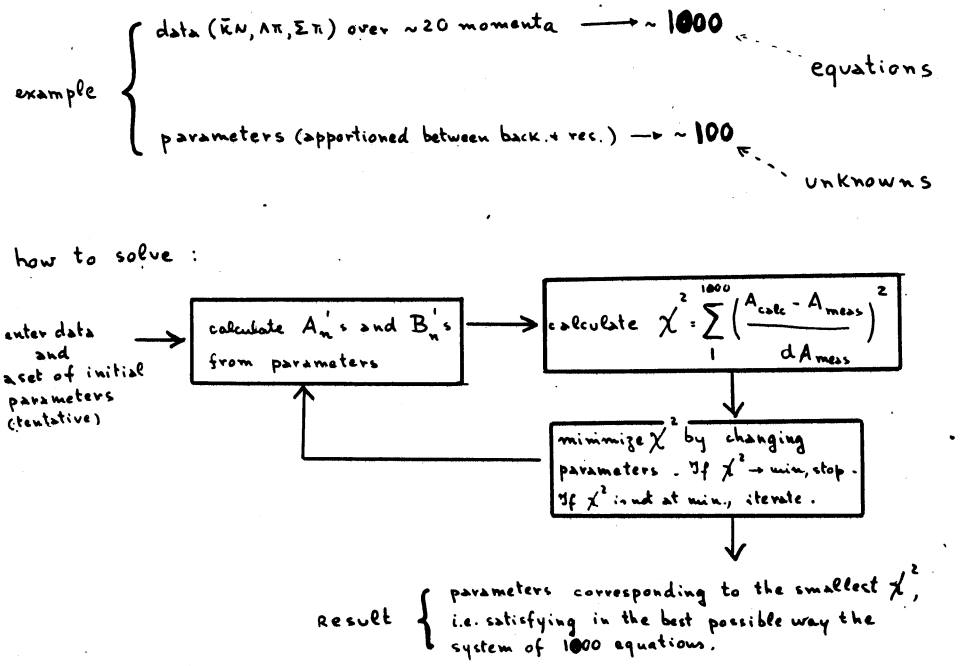
example
data ($\bar{K}N, \Lambda\pi, \Sigma\pi$) over ~20 momenta → ~1000
equations
parameters (apportioned between back.+ res.) → ~100
unknowns
how to solve :
enter data and a set of initial parameters (tentative)
calculate A_n's and B_n's from parameters
calculate $\chi^2 = \sum_1^{1000} \left(\frac{A_{calc} - A_{meas}}{dA_{meas}} \right)^2$
minimize χ^2 by changing parameters. If $\chi^2 \to$ min, stop. If χ^2 is not at min., iterate.
Result
parameters corresponding to the smallest χ^2, i.e. satisfying in the best possible way the system of 1000 equations.

Fig. 44

method or other approaches. Without going into the details of the computer search and of the various combinations of resonant and background waves attempted, it suffices to say that the system of equations can indeed be satisfactorily solved and the minimum $-\chi^2$ found to be in good agreement with that expected. This shows that the parametrization employed, with all its approximations and arbitrariness, is an acceptable representation of what is going on in reality.

Let us now look at the results. Fig. 45 shows how the two elastic channels are fitted under the above conditions. The total cross section (not shown) is also fitted simultaneously. This example, referring only to the elastic amplitudes[1], gives a minimum $-\chi^2$ of 350 for 346 data points and 39 free parameters, i.e. a confidence level of better than 1 part in 20. The partial waves corresponding to the above solution are shown in fig. 46 together with results of other experiments[9,18]

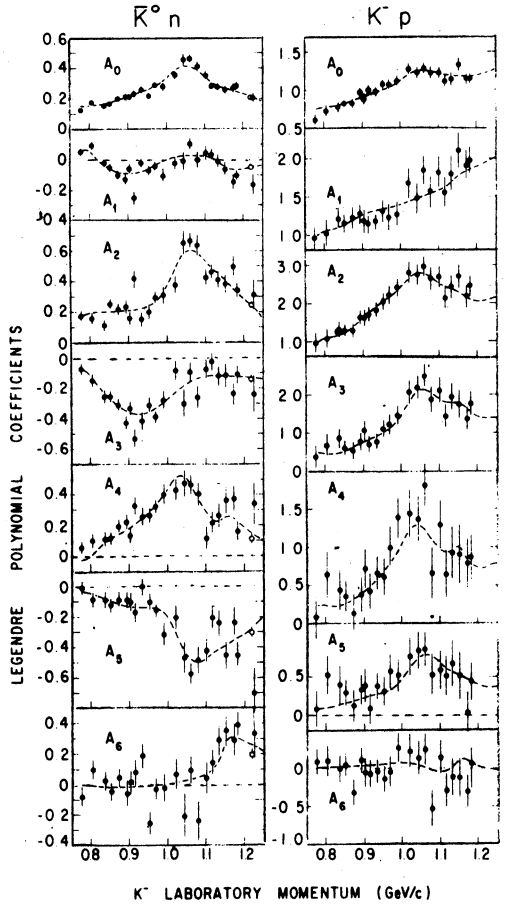

Fig. 45

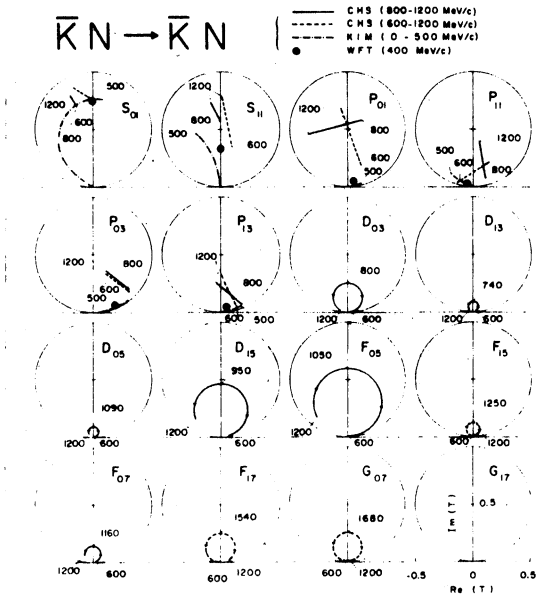

Fig. 46

Figs. 47 and 48 show the amplitudes obtained from the analysis of the other channels. An overall fit to all the channels at once ($\bar{K}N$, $\Lambda\pi$, $\Sigma\pi$) has also been performed with results in good agreement with those of the separate fits[12].

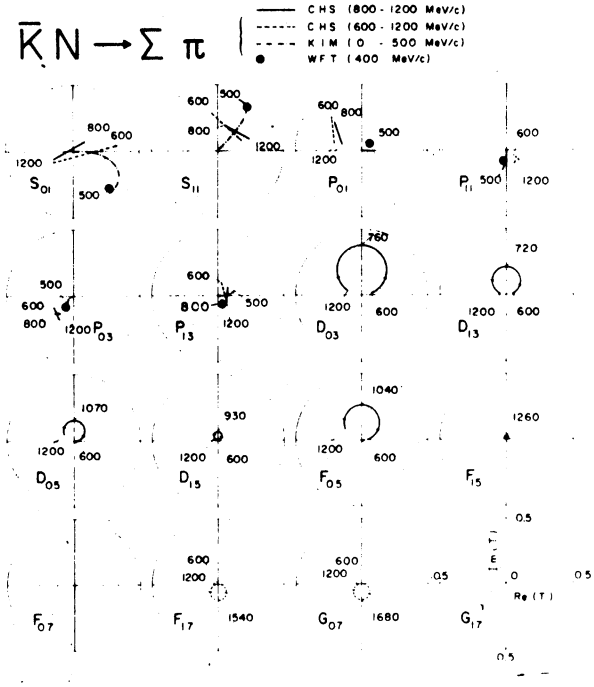

Fig. 47

Before leaving the subject, it should be pointed out that the successful outcome of the above approach may be attributed, in great part, to the relative simplicity of the region examined. The partial waves are present in limited numbers and their behaviour as a function of energy is apparently not very peculiar. That the same approach should also be valid at other (higher) momenta remains to be seen. As an example,

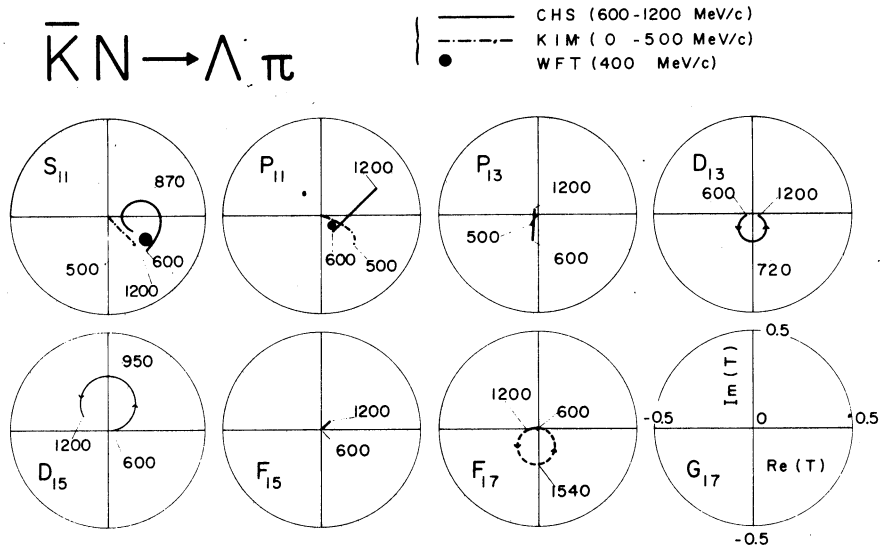

Fig. 48

fig. 49 shows the total $\bar{K}N$ cross section between 2 and 3 GeV/c[19]. The resonant enhancements are here minuscule when compared to those near 1 GeV/c.

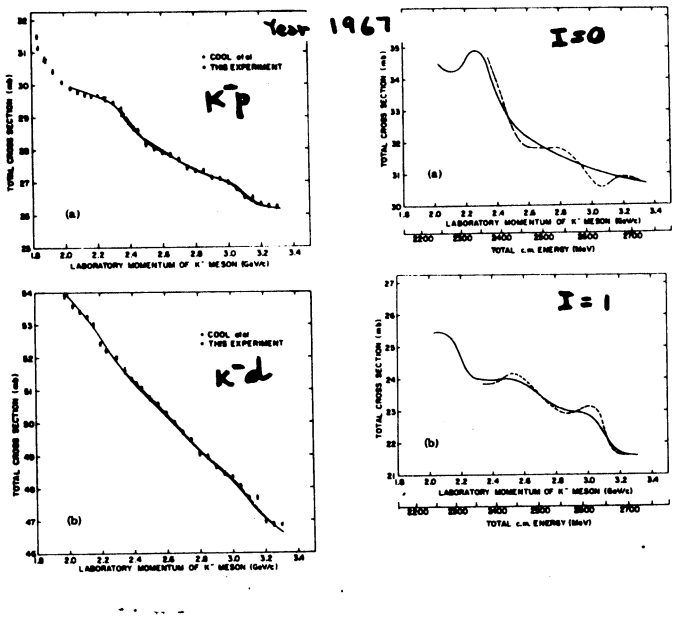

Fig. 49

Furthermore, one knows that partial waves up to J = 11/2 and higher are definitely important at these momenta[20,21]. Last, but not least, the considerable decrease in cross section for all the important two-body channels has the practical effect of reducing the statistics available in reasonably economic experiments.

VI. Partial wave analysis of the pion-nucleon system

As compared to the $\bar{K}N$, a study of the πN system at equivalent energies is in principle much easier. First of all, pions have been around much longer than kaons and their low energy interaction has had the time to be studied extensively and conclusively. Then, they are considerably cheaper than kaons, thus affording better and more detailed measurements. Finally, they are much less prolific than kaons as for possible final states. The above reasons (and others) have substantially contributed to the advanced state of the partial wave analysis of this system and, consequently, of

the knowledge of baryon resonances with S = 0.

Fig. 50 summarizes the state of these resonances; all candidates have been plotted even if in some cases (open circles) there is uncertainty

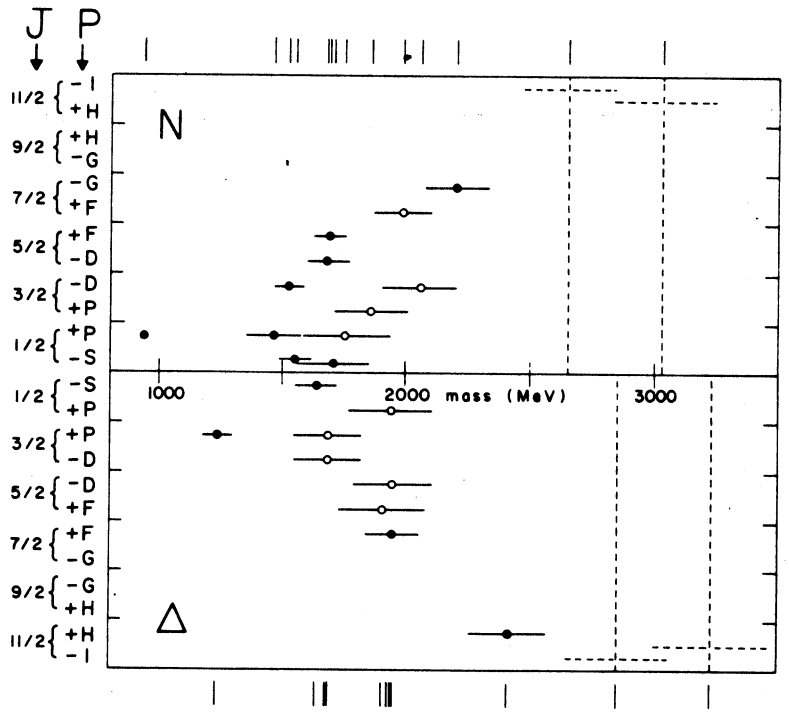

Fig. 50

about their existence. Figs. 51 and 52 illustrate the experimental situation showing, by way of example, a compilation of the total cross sections[22]. Differential cross sections of the elastic channels have also been measured and with comparable accuracy. Finally, polarization measurements have been performed over quite a large range of momenta, as shown in fig. 53[23]. It should be pointed out that the great majority of the data collected has been obtained via counter experiments.

Let us see now what has been done for the partial wave analysis of this system. Only the elastic channel has been thoroughtly analysed, the study of inelastic processes like ΛK, ΣK, etc... being still in a very early

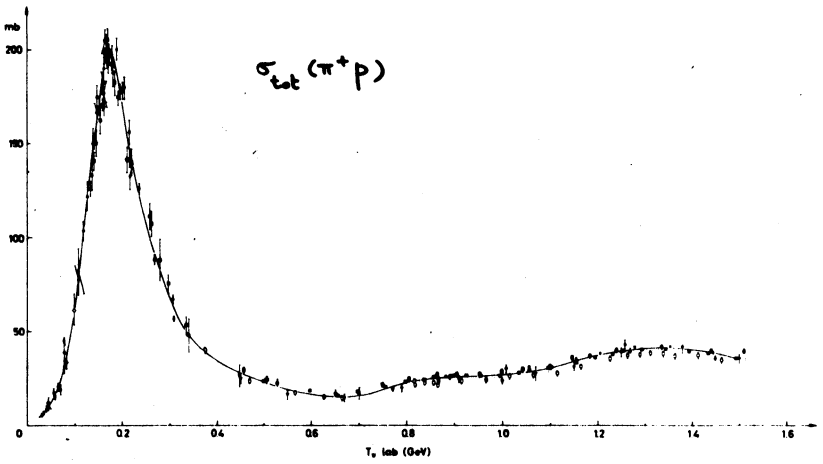

Fig. 51

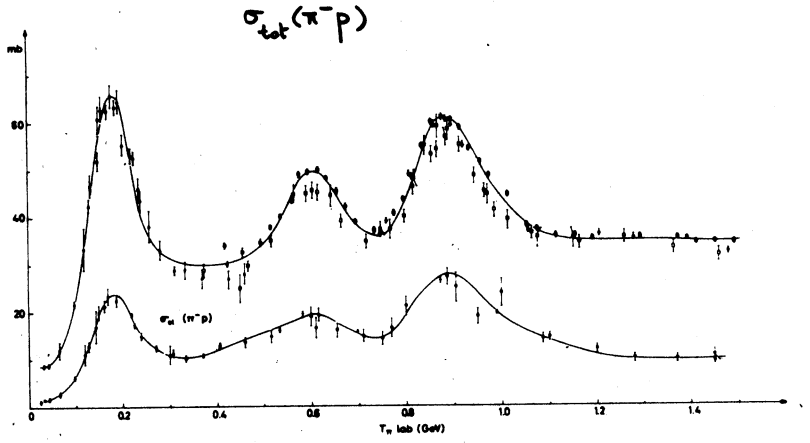

Fig. 52

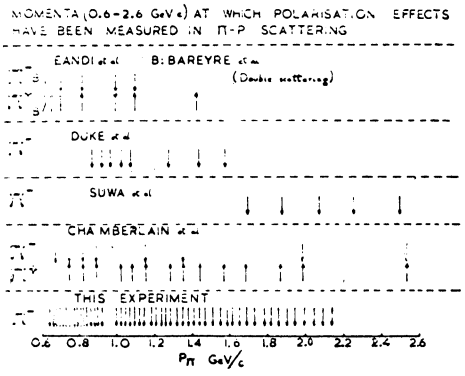

Fig. 53

stage. The main difference with respect to the $\bar{K}N$ system is that here we have enough data at each momentum setting to afford an energy-independent partial wave analysis. Without going into a detailed description of the unknown quantities and the available equations, it is enough to say that the knowledge of polarization, total cross section and differential cross sections for the elastic channels available in $\pi^+ p$ and $\pi^- p$ scattering provides us with an overconstrained system of equations. At each momentum this system can be solved using methods of the same type as those mentioned for the $\bar{K}N$ case. One usually ends up with several solutions (i.e. several sets of partial waves which fit equally well our system of equations) for each one of the momenta considered. Up to this point the method is more or less general; the only differences which exist in practice between the various analyses are on the way in which the data are chosen or the particular procedure adopted to obtain the fitted amplitudes. From here on, instead, there is more freedom as to what to do. The problem is that, having a set of possible solutions, we must decide which is the good one.

Fig. 54 outlines the simple procedure used in the first analysis of this type which successfully yielded a wealth of unexpected new

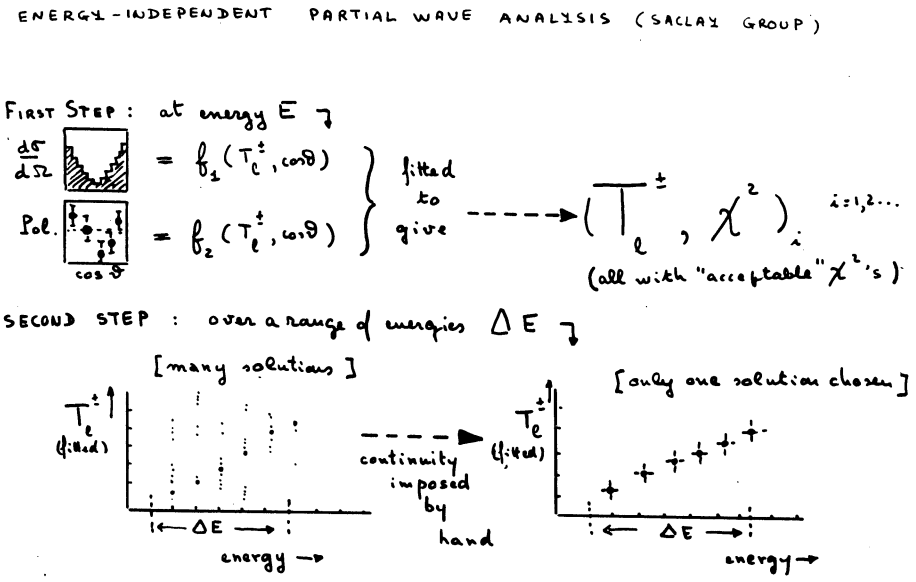

Fig. 54

resonances[24]. The good solutions are here chosen by requiring that they satisfy the maximum possible "continuity" as a function of energy. How to define this "continuity" is of course the problem. This was solved by hand (or rather by eye) in the analysis of ref. 24; referring to fig. 54, one should keep in mind that the operation of smoothing out the energy dependence of the amplitudes must be done simultaneously over <u>all</u> amplitudes (each one of them represented by two quantities: phase shift and absorption parameter or, alternatively, real and imaginary part). Thus one should imagine that the plot of $T_\ell^\pm$ vs E in fig. 54 represents in reality a whole series of graphs where each point corresponds to another point in a different graph. A certain degree of arbitrariness is undoubtedly implicit in this procedure; on the other hand, the absence of any particular model for the energy dependence of the amplitudes (what one could call a "theoretical prejudice") may well compensate for the above subjectivity. Fig. 55 shows some of the results of this analysis. The points (if one can see them) represent the amplitudes chosen at each energy; the curves are an additional smoothing out of the results, suggesting the most likely trajectory described by the amplitudes as a function of energy.

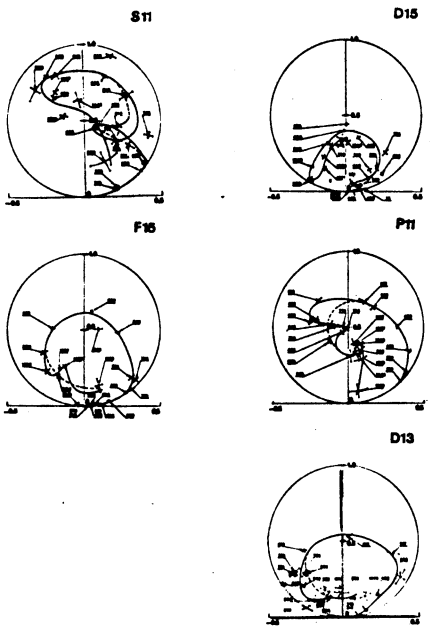

Fig. 55

The arbitrariness mentioned above can be somewhat reduced if a more impartial computer-controlled method is introduced at the "second step" of fig. 54 when imposing continuity. This has been done in another analysis[23] which otherwise is not very different from the preceding one. The continuity criterion takes the form of a "shortest possible path" over a certain energy interval, of conditions on the derivatives between adjacent energy settings, etc. Fig. 56 shows one of the resulting amplitudes. As compared to the

same in fig. 55 the points are less scattered but the curve is almost identical.

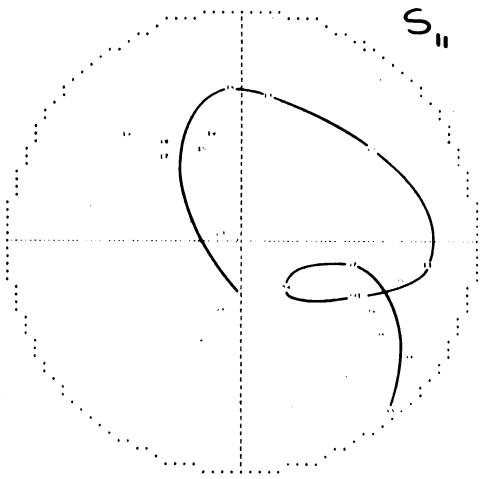

Fig. 56

Let us now examine a different and more sophisticated approach to the problem of selecting our good solutions. Instead of simply requiring a smooth energy dependence of the amplitudes without invoking any specific pattern, one can demand that the energy dependence should be such as to satisfy in the best possible way certain conditions between the real and imaginary part of the amplitudes called "dispersion relations". A discussion of dispersion relations is well outside the scope of the present lectures; a good place to find a description of this technique, particularly in connection with partial wave analysis, is the series of lectures of ref. 25. Fig. 57 gives a very sketchy summary of the

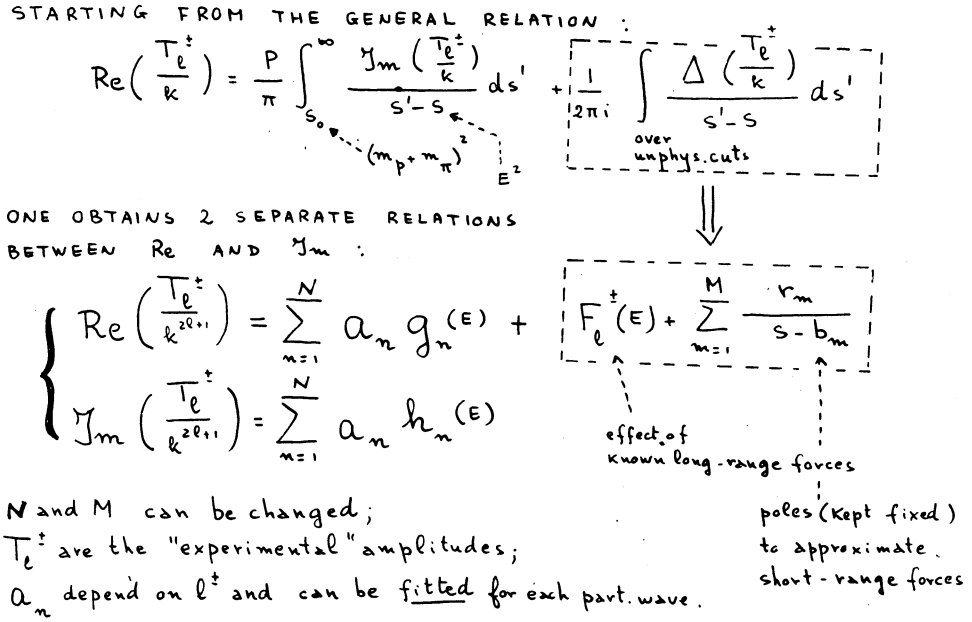

Fig. 57

formulae used in the analysis of ref. 26. The main point is that from the general expression (which does not have a form that can easily be exploited for the purpose mentioned above) one obtains, through the magic of something called "conformal mapping", two expressions valid separately for the real and imaginary part of the amplitudes[25]. The $g_n(E)$ and $h_n(E)$ in these expressions are known functions of the energy and the summation over n, which in principle should go to ∞, can be truncated at some value N. The summation over "poles" is also finite, with M usually small. The early arbitrariness in energy dependence is now reduced (not eliminated) and, in addition, a connection is established between the previously uncorrelated real and imaginary part of each amplitude.

All this wealth of fresh information does not come completely free, of course. Without raising doubts as to the basic validity of dispersion relations, their practical use does necessarily imply a series of approximations, assumptions and other mundane involvements which can indeed be questioned. Thus, for example, one may have preferred more (or less) poles, a different order of approximation in the sum over n, a stronger (or weaker) effect of the long-range forces, etc... All this should not be taken as a detraction of the method but rather as a warning against possible biases which (just because they are much more subtle than those of the rudimentary procedures described previously) may indeed still linger on even in these aseptic surroundings.

Fig. 58 shows schematically what may have been the approach used in this method[26] (no official detailed description is available as yet). What is referred to as "free parameters" are the coefficients a_n of fig. 57; the "order of complexity" refers to the number of coefficients (N) and poles (M). The "iteration" procedure involves the re-calculation of the amplitudes directly from the data starting each time from the previously obtained "corrected" amplitude $T_{corr.}$ and its error.

The results, shown as solid curves in fig. 59, are spectacular. All

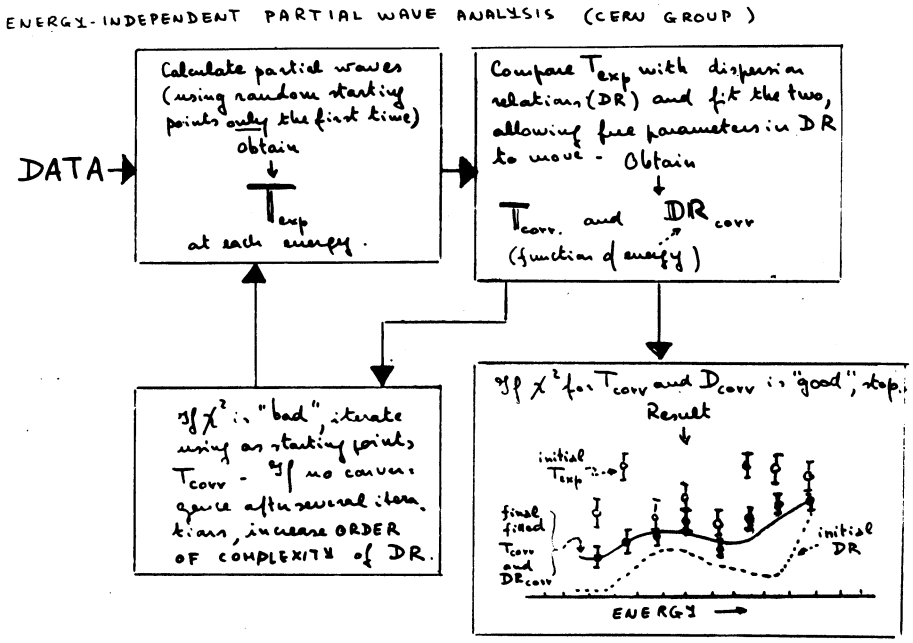

Fig. 58

the inaesthetic wiggles of the previous solutions have disappeared and, if nature is indeed smooth, there is no doubt that this is the smoothest representation. Still, it may be that in some case the solutions are <u>too</u> smooth . As in the case of S_{11}, which can be compared with that in figs. 55 and 56: the small secondary loop is gone. Perhaps it shouldn't.

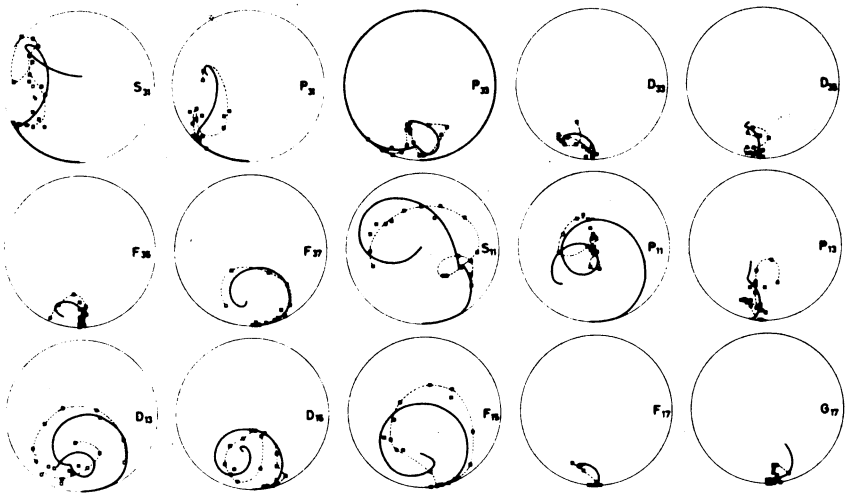

Fig. 59

On the other hand, the procedure seems to be very valuable when trying to make sense of small amplitudes. Thus, for example, look at D_{33} in fig. 60. Here the open circles are from the best solution of ref. 24 ; there is little doubt that the full circles and the curves (from ref. 26) make more sense than the former. Similarly, one can see in fig. 61 a collection of small amplitudes[24] where the first approach (solid curves) would demand such an erratic behaviour that one is instinctively tempted in trusting the more dignified path described by the second approach (dotted curves). All this, if correct, would speak very much in favour of the second method in spite of its added complications and possible biases.

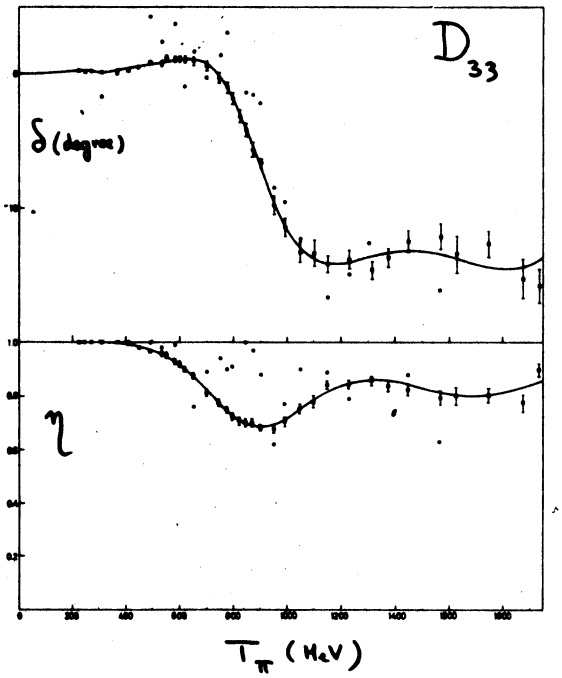

Fig. 60

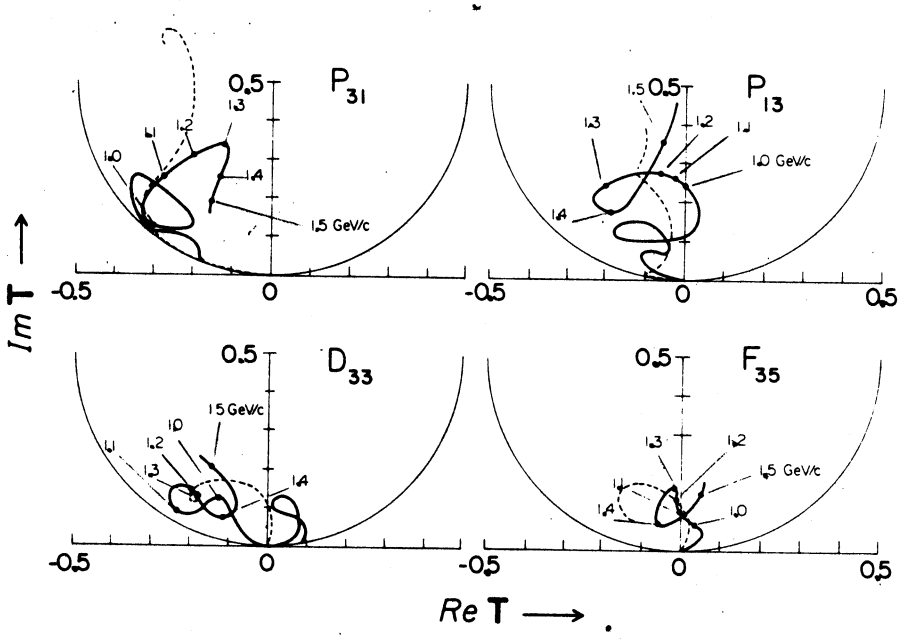

Fig. 61

THIRD LECTURE

VII. Applications to SU(3)

Now that we know how and where to look for baryon resonances, we may perhaps wonder why we are doing it and whether it is really worth the effort. So many of them already exist on the market that the mere pleasure of a search and analysis may not be a reward by itself any more. We may then go one step further and try to see if the theoretical models that have been proposed make sense or not. This, of course, could have been done much earlier (and indeed it was[27]) but it is only at present that we dispose of a sizeable body of information and that meaningful tests can be done.

The simplest level of model predictions is offered by SU(3). I will assume here that everybody is already familiar with at least the more fundamental aspects of this theory. In what follows we shall concentrate on the existence and requirements of the baryon "multiplets": how many can be made up, what is their composition and how well do the branching fractions of their members agree with the predictions. This lecture follows very closely the articles of ref. 28.

A multiplet is usually proposed when a sufficient number of particles is found, all with the same J^P and with masses such as to obey, within broad limits, some so-called "mass law". Corrections on the mass values deriving from "mixing" with other multiplets are sometimes taken into account. Finally, one can check that the decay modes of the members of the multiplet are in agreement with the assumption that there is only <u>one</u> "coupling constant" characteristic of the multiplet in question. It is particularly the latter point which is worth insisting upon; indeed, the fact that a mass happens to be correct may well be a coincidence due to the large variety of resonances existing throughout the mass spectrum.

An additional self-consistency check, which is quite useful in this

identification procedure, is offered by the different decay modes that the same resonance can have. Let us see, for example, what this means. We are already familiar with the isotopic spin requirements for the various charge combinations of the same decay mode of a resonance. Thus, for example, an I = 0 resonance decaying into $\Sigma\pi$ will distribute itself equally into $\Sigma^+\pi^-$, $\Sigma^0\pi^0$, $\Sigma^-\pi^+$; an I = 1 resonance will not go into $\Sigma^0\pi^0$, etc... The relative rates are given by Clebsch-Gordan coefficients, as everybody knows. What is less evident (and indeed it demands the validity of SU(3) and the attribution to a definite multiplet) is that one can also do the same calculation to see how many times for example, the resonance decays into $\Sigma\pi$ and how many times into $\Lambda\pi$. The relative importance of the various decay modes are given by Clebsch-Gordan coefficients of SU(3), which are available in several tabulations (for example in ref. 29 and 30). These coefficients, on the other hand, do not tell us the whole story. We must remember that the particles into which the resonances decay may have masses quite different from each other; so we must introduce a "phase space" factor to take this into account. Furthermore, when the orbital angular momentum of the system is different from zero, there will be centrifugal barrier effects which must also be considered.

All this is explicitly written out in fig. 62, which gives the formula

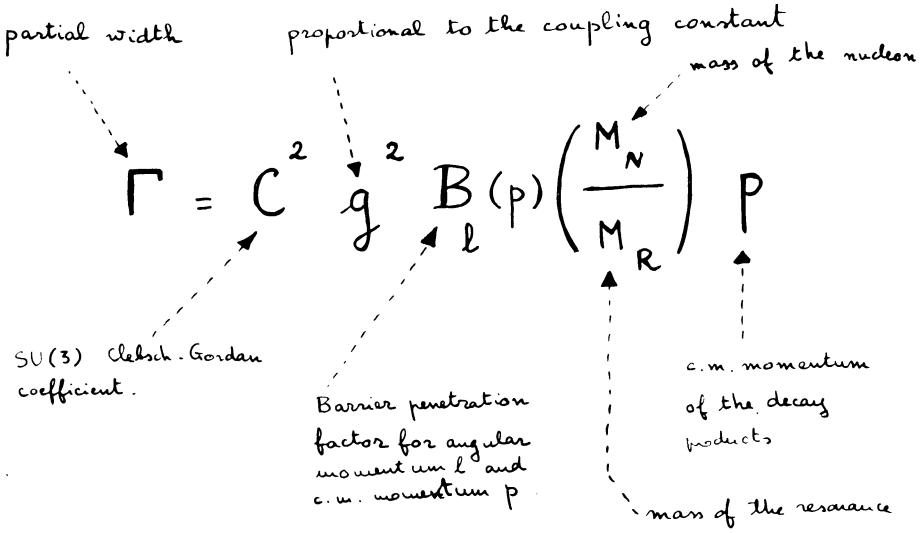

Fig. 62

used in ref. 28 for the case of singlets and decuplets. The partial width Γ measures the rate of a certain decay mode, p is the phase space factor, B_ℓ is the centrifugal barrier factor of fig. 29, (M_N / M_R) is put in to normalize things. The factor g^2 we can call "coupling constant" and it is this which should remain constant for all the members of the same multiplet.

Fig. 63 shows the Clebsch-Gordan coefficients for the most familiar decay modes of hyperon resonances[30]. Here the symbol Y stands for hypercharge (B + S), I and I_3 for magnitude and third component of the isotopic spin.

SOME CLEBSCH-GORDAN COEFFICIENTS OF $\{8\}\otimes\{8\}$ going into:

example	$y\ i\ i_3$ $\quad y'\ i'\ i'_3$	$\{10\}$	$\{1\}$
		0	0 $\quad$ Y
		1	0 $\quad$ I
		0	0 $\quad$ I_3
$p\,K^-$	$1\ \frac{1}{2}\ \frac{1}{2}$ $\quad -1\ \frac{1}{2}\ -\frac{1}{2}$	$-\sqrt{1/12}$	$\sqrt{1/8}$
$n\,\bar{K}^0$	$1\ \frac{1}{2}\ -\frac{1}{2}$ $\quad -1\ \frac{1}{2}\ \frac{1}{2}$	$-\sqrt{1/12}$	$-\sqrt{1/8}$
$\Sigma^+\pi^-$	$0\ 1\ 1$ $\quad 0\ 1\ -1$	$\sqrt{1/12}$	$\sqrt{1/8}$
$\Sigma^0\pi^0$	$0\ 1\ 0$ $\quad 0\ 1\ 0$	0	$-\sqrt{1/8}$
$\Sigma^0\eta$	$0\ 1\ 0$ $\quad 0\ 0\ 0$	$\sqrt{1/4}$	0
$\Sigma^-\pi^+$	$0\ 1\ -1$ $\quad 0\ 1\ 1$	$-\sqrt{1/12}$	$\sqrt{1/8}$
$\Lambda\pi^0$	$0\ 0\ 0$ $\quad 0\ 1\ 0$	$-\sqrt{1/4}$	0

Fig. 63

Let us now make a tour of the most reliable multiplets and see if and how the relation in fig. 62 is satisfied in practice. In fig. 64 we see the well-known $3/2^+$ decuplet and a rather hypothetical $7/2^+$ decuplet which, through some stretch of imagination, can also be thought of as the Regge-recurrence of the first. The numbers given as branching fractions (in this and the following figures) come out only partly from ref. 2; full details can

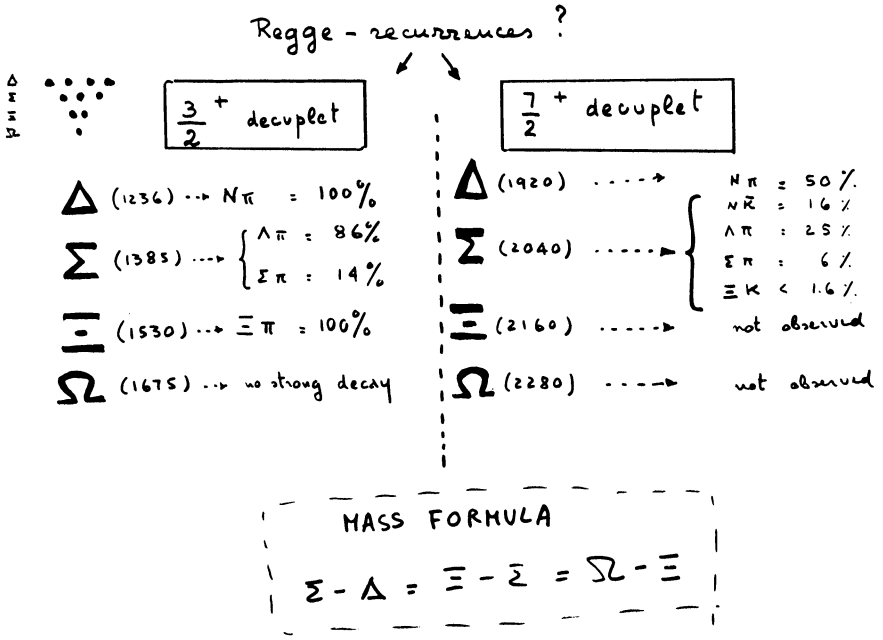

Fig. 64

be found in ref. 28. The most likely candidates for singlets are those in fig. 65 (a possible choice for Regge-recurrences) plus Λ(1405) with its main decay mode into Σπ.

Now, instead of contemplating the above arrangements and congratulating ourselves for having found so many resonances with the correct spin-parity

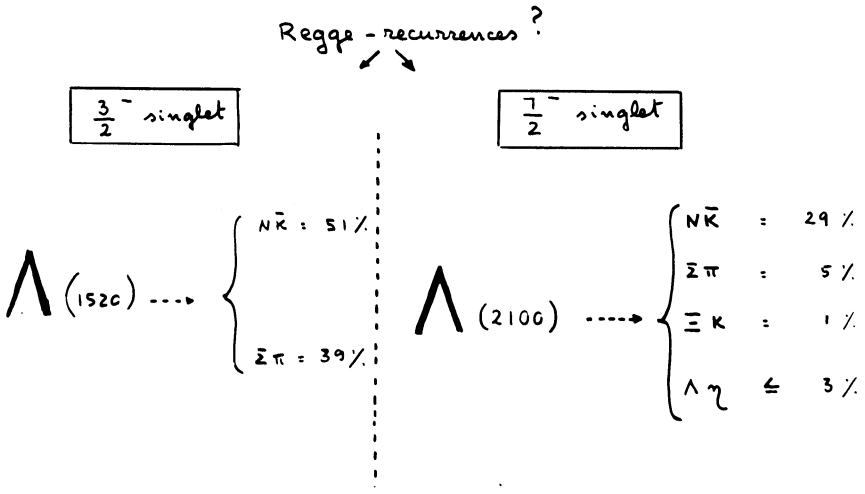

Fig. 65

and mass value, we can do something more and see if the 16 branching fractions associated with these resonances make sense or not. This is shown in fig. 66 where the value of g^2 (and its error) as obtained through the formula in fig 62 is plotted for each one of the above decay modes. Right away we can see that, even taking into account the errors, there are serious discrepancies between the values of g^2 inside each multiplet. Even

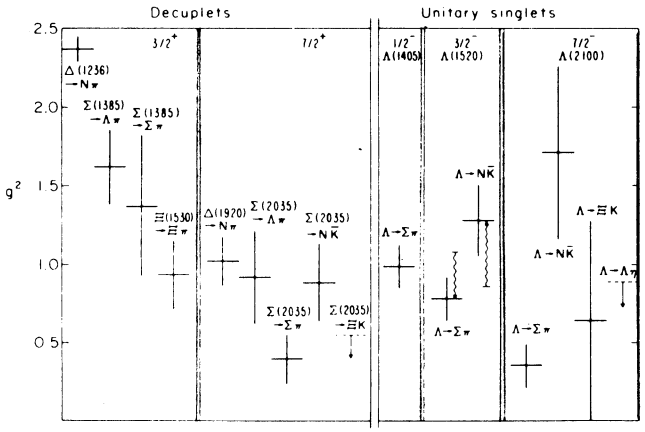

Fig. 66

the $3/2^+$ decuplet, that most respectable and famous multiplet, gives values of g^2 differing as much as a factor 2. It is clear that if we start questioning also <u>this</u> multiplet, then we may as well give up the whole idea and do something else. Instead, let us blame ourselves for the inadequate connection between Γ and g^2 and let us consider discrepancies of this order of magnitude as unavoidable and quite acceptable. Having thus broadened our tolerance, we can then inspect fig. 66 with a different eye. The coupling constants are in satisfactory agreement within multiplets and actually even between <u>different</u> multiplets. This agreement is certainly not trivial and we are then encouraged to proceed with our simple formula towards more questionable multiplets.

In order to do so, and having exhausted all the reasonably well-established singlets and decuplets, we must modify slightly the previous

formula so as to adapt it to the octet case. Fig. 67 recalls that there are two possible octets to be considered and that what one sees in reality is a mixture of the two. Thus the expression relating the coupling constant to

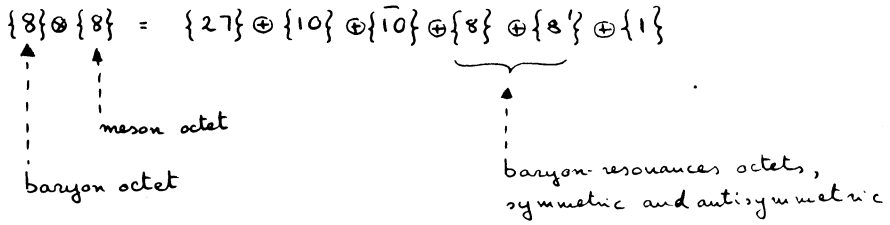

In general, the observed baryon-resonances octets will be linear combinations of {8} and {8'} :

$$\psi = \psi_{\{8\}} \cos\vartheta + \psi_{\{8'\}} \sin\vartheta$$

mixing parameter defined as ----► $\alpha^{-1} = 1 + \frac{\sqrt{5}}{3} \operatorname{tg}\vartheta$

Fig. 67

the observed partial width must now contain a linear combination of the coupling constants (g_d and g_f) for the two octets. Fig. 68 shows the new

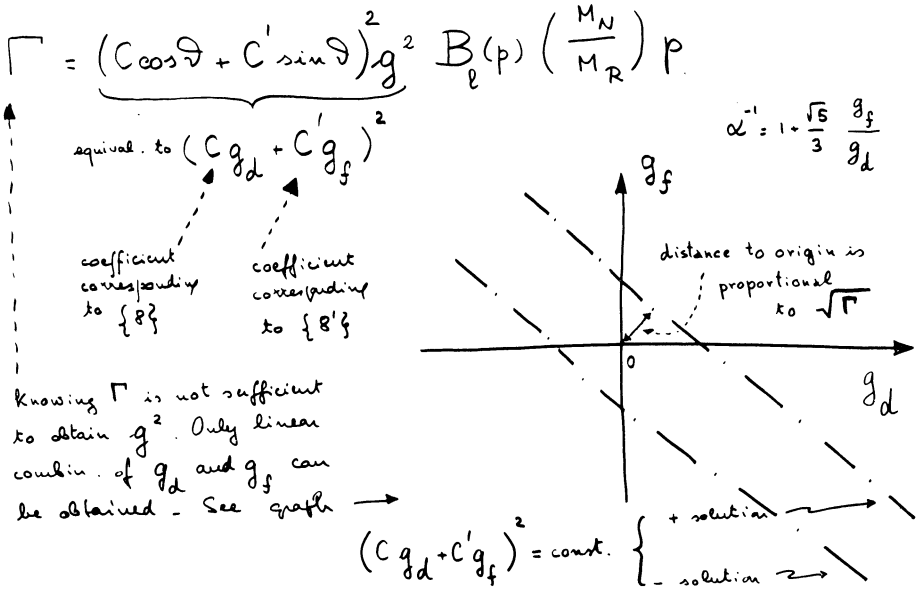

Fig. 68

expression and how, from it, one can only obtain a set of straight lines in the g_d, g_f plane. The knowledge of only one partial width is clearly insufficient for determining g_d and g_f separately. On the other hand, if more partial widths are available, the problem can be solved (or better "fitted", because at a certain point there will be more constraints than unknowns). Alternatively, when this occurs, we have a way of knowing if the members of the octet in question were indeed well matched. The probability that this could happen by chance for a random set of resonances is admittedly very remote.

Let us now see if all this works in practice. Fig. 69 gives some examples of Clebsch-Gordan coefficients valid for the octets, again from

SOME CLEBSCH-GORDAN COEFFICIENTS

OF $\{8\}\otimes\{8\}$ going into:		$\{8\}$	$\{8'\}$	$\{8\}$	$\{8'\}$	
		0	0	0	0	Y
example	$y\ i\ i_3$ $y'\ i'\ i'_3$	1	1	0	0	I
		0	0	0	0	I_3
$p\ K^-$	$1\ \frac{1}{2}\ \frac{1}{2}$ $-1\ \frac{1}{2}\ -\frac{1}{2}$	$-\sqrt{3/20}$	$\sqrt{1/12}$	$\sqrt{1/12}$	$\sqrt{1/4}$	
$n\ \bar{K}^0$	$1\ \frac{1}{2}\ -\frac{1}{2}$ $-1\ \frac{1}{2}\ \frac{1}{2}$	$-\sqrt{3/20}$	$\sqrt{1/12}$	$-\sqrt{1/20}$	$-\sqrt{1/4}$	
$\Sigma^+\pi^-$	$0\ 1\ 1$ $0\ 1\ -1$	0	$\sqrt{1/3}$	$-\sqrt{1/5}$	0	
$\Sigma^0\pi^0$	$0\ 1\ 0$ $0\ 1\ 0$	0	0	$\sqrt{1/5}$	0	
$\Sigma^0\eta$	$0\ 1\ 0$ $0\ 0\ 0$	$\sqrt{1/5}$	0	0	0	
$\Sigma^-\pi^+$	$0\ 1\ -1$ $0\ 1\ 1$	0	$-\sqrt{1/3}$	$-\sqrt{1/5}$	0	
$\Lambda\pi^0$	$0\ 0\ 0$ $0\ 1\ 0$	$\sqrt{1/5}$	0	0	0	

Fig. 69

ref. 30. Figs. 70 and 71 illustrate the case of the $1/2^-$ nonet. Those branching fractions which have been measured appear to be in rather good agreement with the predictions of a single d and f coupling constant. This is indicated by a common crossing area (the dark spot of fig. 71) in the

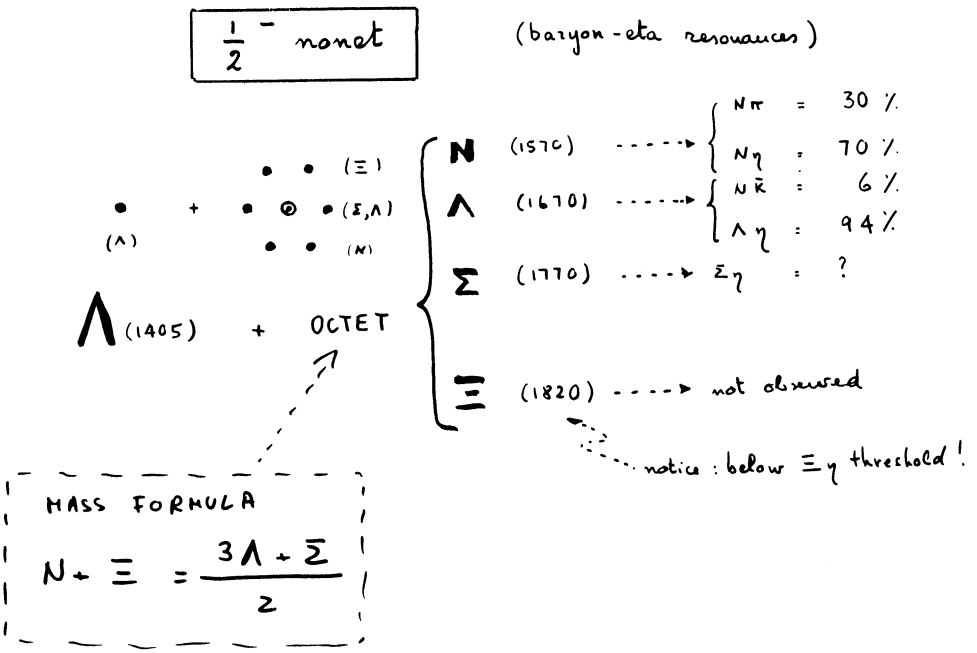
1/2⁻ nonet
(baryon-eta resonances)
(Ξ)
(Σ,Λ)
(N)
(Λ)
Λ (1405) + OCTET
N (1570) ----> Nπ = 30 %
Nη = 70 %
Λ (1670) ----> NK̄ = 6 %
Λη = 94 %
Σ (1770) ----> Ση = ?
Ξ (1820) ----> not observed
notice : below Ξη threshold !
MASS FORMULA
N + Ξ = (3Λ + Σ)/2

Fig. 70

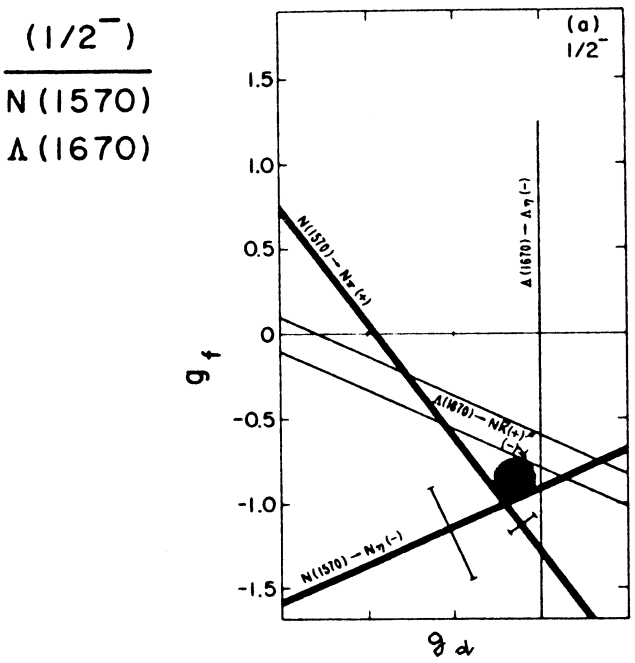
(1/2⁻)
N(1570)
Λ(1670)
(a)
1/2⁻
1.5
1.0
0.5
0
-0.5
-1.0
-1.5
g_f
g_d
N(1570) – Nπ(+)
Λ(1670) – Λη(-)
Λ(1670) – NK̄(+)
(-)
N(1570) – Nη(-)

Fig. 71

g_d, g_f plane. The bars across the straight lines indicate the uncertainty due to the experimental input. The convention followed throughout is that the thinner a line is, the more uncertain is the corresponding branching fraction.

Figs. 72 and 73 show the situation of what is currently believed to

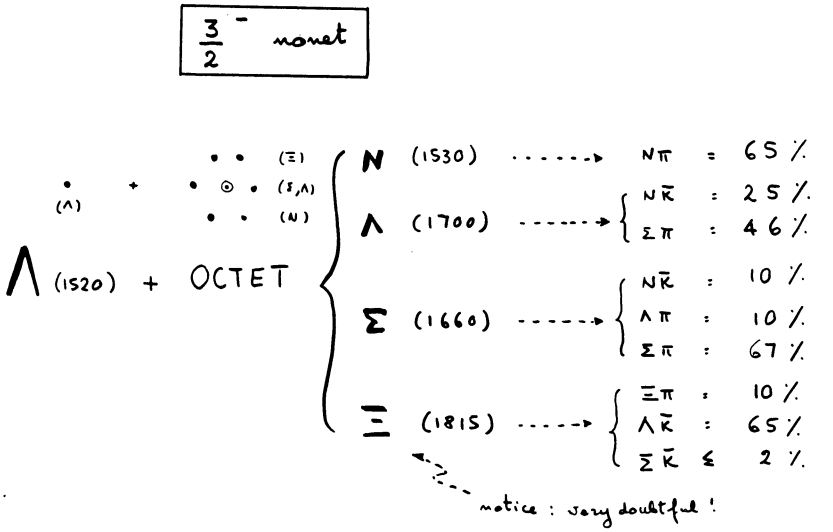

Fig. 72

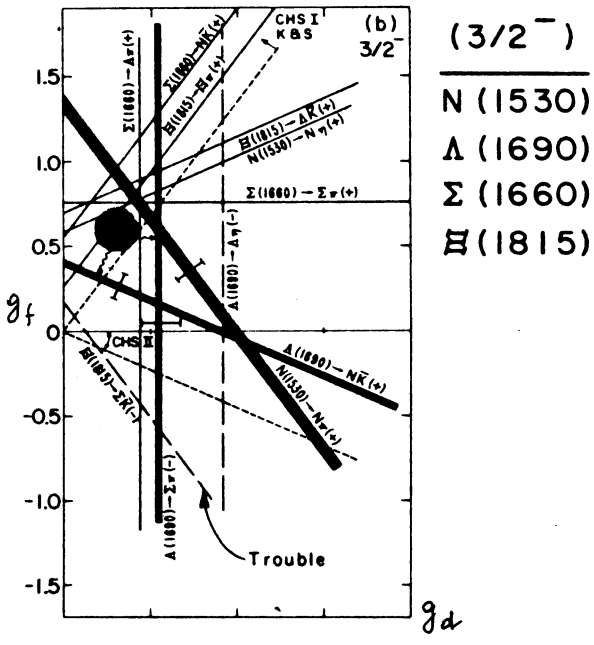

Fig. 73

be the $3/2^-$ nonet. There are problems here (see ref. 28 for details) but a reasonable crossing area can still be found. A valid question, at this point, is how sure can one be that the crossing area is where it has been drawn and not somewhere else. As it is evident from fig. 73, there are other possibilities which are not necessarily less likely than the one chosen. There is not much of an answer to this, except that, when more and more accurate branching fractions become known, then the above uncertainty is guaranteed to disappear. This, however, brings up another point which is of interest in the choice of the crossing area. The dotted lines labelled CHS or KS in fig. 73 mark the boundaries of the allowed crossing regions; that is, only a part of the g_d, g_f plane is available for this region and we can exploit this constraint when trying to decide between alternative choices.

How this comes about is detailed in ref. 31. Until now we have never considered the information conveyed by the phase of an inelastic amplitude at resonance. Remember fig. 25, where we saw that the elastic amplitude at resonance is purely imaginary and positive, whereas the inelastic amplitude can be either positive or negative. This means that the phase of the inelastic amplitude with respect to the elastic can be either 0^o or 180^o. This can be immediately related to the sign of the product of the elastic and the inelastic coupling constants as shown in fig. 74. Now, if we have a way of measuring the relative phases of a set of resonances (and this comes out from the analyses discussed in the second lecture) and if one of these resonances happens to require a definite sign for the product of its coupling constants, then we also have a useful inequality on the coupling constants for the resonances in question. Referring to fig. 75, we see that from the relative phase of the $\Lambda\pi$ decay mode of certain resonances we can limit the allowed region of the g_d, g_f plane to the shaded areas[31]. In the same way, the $\Sigma\pi$ decay mode of these and other resonances contributes the information collected in fig. 76[28]. It is from these considerations that one produces the dotted boundary lines in fig. 73 and following.

What can be obtained from the relative phase at resonance between two resonances :

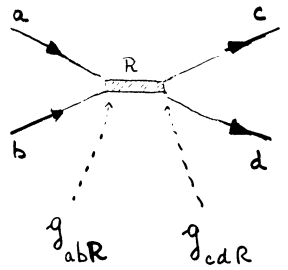

$$T_{ab\to cd} = \frac{g_{abR} \cdot g_{cdR}}{(E_R - E) - i\frac{\Gamma}{2}}$$

For example, $\bar{K}N \to \bar{K}N$ and $\bar{K}N \to \Lambda\pi$ through Y^* gives :

- elastic channel amplitude $\propto g^2_{\bar{K}NY^*}$ ◄---- always positive
- $\Lambda\pi$ - channel amplitude $\propto g_{\bar{K}NY^*} \cdot g_{\Lambda\pi Y^*}$ ◄---- its sign defines the allowed regions of the g_d - g_f plane.

Fig. 74

From the relative phase at resonance in $\bar{K}N \to \Lambda\pi$.

Resonances observed	$\Sigma(1660)$	$\Sigma(1760)$	$\Sigma(1910)$	$\Sigma(2030)$
Phase at resonance	⇧	⇩	⇩	⇧
Multiplet assignment	$\frac{3}{2}^-$ octet	$\frac{5}{2}^-$ octet	$\frac{5}{2}^+$ octet	$\frac{7}{2}^+$ decuplet
Sign of $g_{\bar{K}NY^*} \cdot g_{\Lambda\pi Y^*}$	+	−	−	+ (must)
Value of ⇧	$\sqrt{\frac{1}{5}}\, g_d \left(-\sqrt{\frac{3}{20}}\, g_d + \sqrt{\frac{1}{12}}\, g_f\right)$			$\sqrt{\frac{1}{48}}\, g^2_{\{10\}}$
Allowed values of g_f and g_d	$g_f > \sqrt{1.8}\, g_d$	$g_f < \sqrt{1.8}\, g_d$		
Allowed region of the $g_d > 0$, g_f plane →	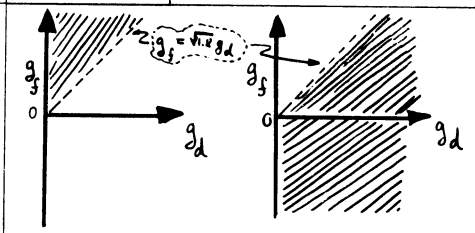			

Fig. 75

From the phases at resonance in $\bar{K}p \rightarrow \Sigma\pi$.

Resonance	Σ (1660)	Λ (1700)	Σ (1760)	Λ (1830)	$\bar{\Sigma}$ (1910)	$\bar{\Lambda}$ (1820)	$\bar{\Sigma}$ (2030)	$\bar{\Lambda}$ (2100)
Phase	$\Uparrow$	$\Downarrow$	$\Uparrow$	$\Downarrow$	$\Uparrow$	$\Downarrow$	$\Downarrow$	$\Uparrow$
Multiplet	$\frac{3}{2}^-$ octet		$\frac{5}{2}^-$ octet		$\frac{5}{2}^+$ octet		$\frac{1}{2}^+$ dec.	$\frac{1}{2}^-$ singl.
Sign and value of $g_{\bar{K}p\Sigma^+} \cdot g_{\pi\Sigma\Lambda^+}$	+	−	+	−	+	−	− (must!)	+ (must!)
	$-\frac{1}{\sqrt{5}} g_d \left(\frac{1}{\sqrt{20}} g_d + \frac{1}{2} g_f\right)$ for Λ's						$-\frac{1}{12} g^2_{\{10\}}$	$\frac{1}{8} g^2_{\{1\}}$
	$\frac{1}{\sqrt{3}} g_f \left(-\sqrt{\frac{3}{20}} g_d + \frac{1}{\sqrt{12}} g_f\right)$ for Σ's							
Allowed regions of the $g_d > 0$, g_f plot ▨	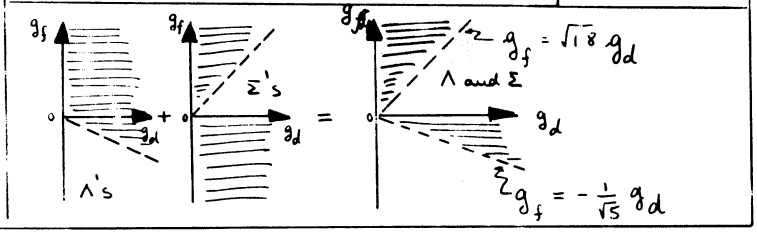							

Fig. 76

The last four figures, from 77 to 80 show the status of the remaining octets. The same type of considerations is valid here as in the previous cases. The detailed discussion of these results is left to ref. 28.

The general conclusion that one derives from this exercise is that, remarkably enough, the bulk of the data examined agrees rather well with the model in question. At the same time there are also discrepancies, here and there, which are serious enough to cast doubts on the correctness of either some specific multiplet composition or the experimental information employed. In all cases the exercise is quite useful. It shows where the experimental information needs a more careful treatment and also provides a guide to which could be the most meaningful experiments to perform in the future.

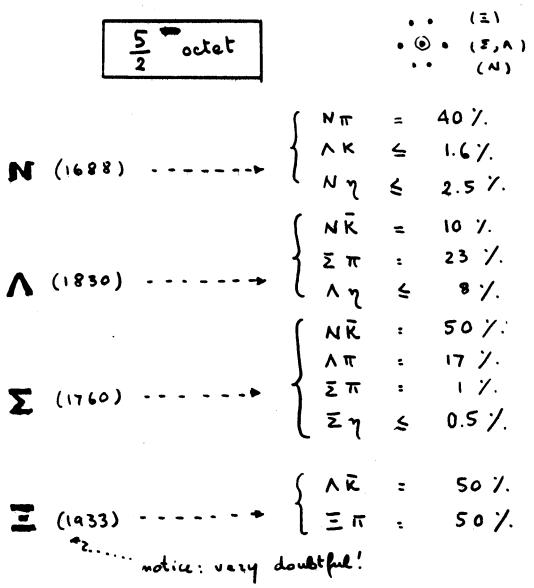
5/2 octet
(Ξ)
(Σ,Λ)
(N)
N (1688) ------->
Nπ = 40 %.
ΛK ≤ 1.6 %.
Nη ≤ 2.5 %.
Λ (1830) ------->
NK̄ = 10 %.
Σπ : 23 %.
Λη ≤ 8 %.
Σ (1760) ------->
NK̄ : 50 %.
Λπ : 17 %.
Σπ : 1 %.
Ξη ≤ 0.5 %.
Ξ (1933) ------->
ΛK̄ = 50 %.
Ξπ : 50 %.
notice: very doubtful!

Fig. 77

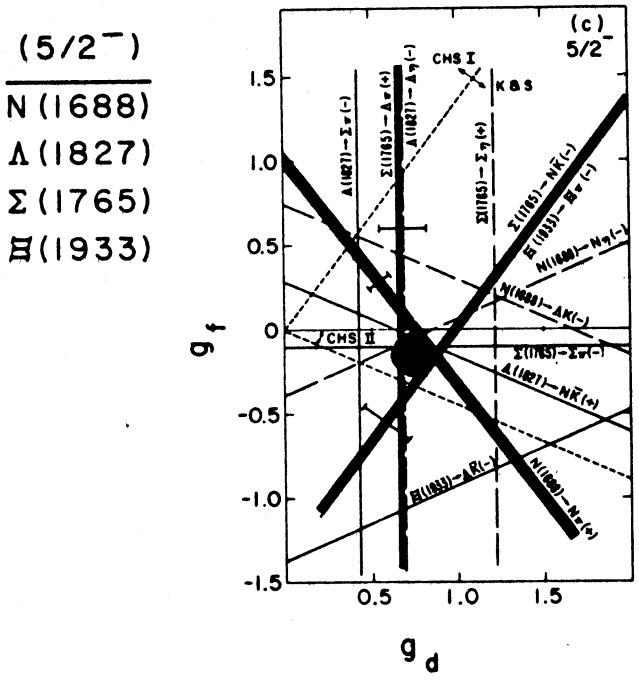
(5/2⁻)
N(1688)
Λ(1827)
Σ(1765)
Ξ(1933)
(c)
5/2⁻
CHS I
KBS
CHS II
1.5
1.0
0.5
0
-0.5
-1.0
-1.5
0.5
1.0
1.5
g_f
g_d

Fig. 78

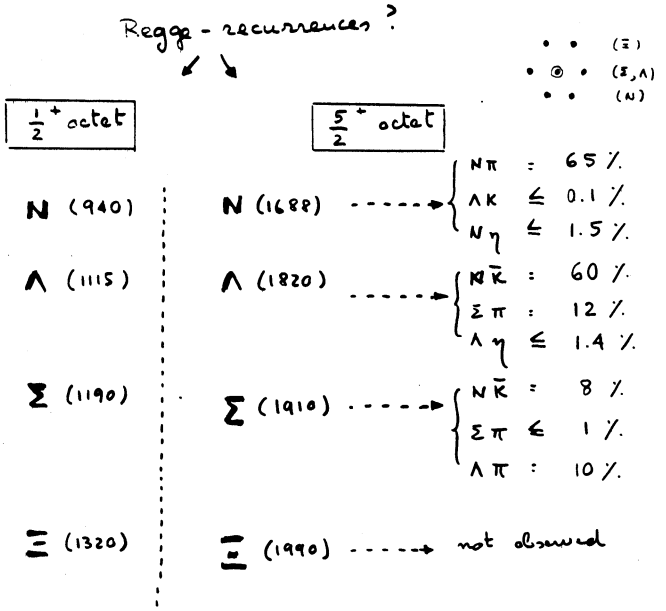
Regge - recurrences ?
(Ξ)
(Σ,Λ)
(N)
$\frac{1}{2}^+$ octet
$\frac{5}{2}^+$ octet
N (940)
N (1688)
Nπ : 65 %
ΛK ≤ 0.1 %
Nη ≤ 1.5 %
Λ (1115)
Λ (1820)
NK̄ : 60 %
Σπ : 12 %
Λη ≤ 1.4 %
Σ (1190)
Σ (1910)
NK̄ : 8 %
Σπ ≤ 1 %
Λπ : 10 %
Ξ (1320)
Ξ (1990)
not observed

Fig. 79

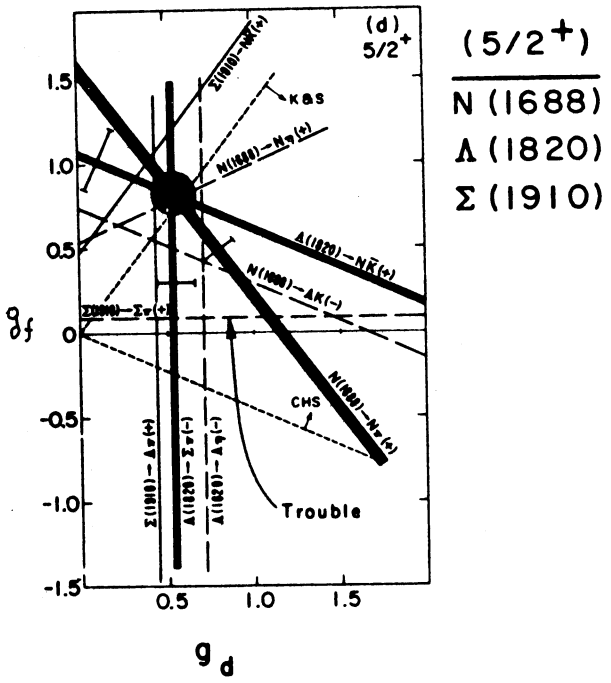
(d)
5/2+
KBS
CHS
Trouble
1.5
1.0
0.5
0
-0.5
-1.0
-1.5
0.5
1.0
1.5
g_f
g_d
(5/2+)
N (1688)
Λ (1820)
Σ (1910)

Fig. 80

References

1. R. Armenteros, M. Ferro-Luzzi, D.W.G. Leith, R. Levi-Setti, A. Minten, R.D. Tripp, H. Filthuth, V. Hepp, E. Kluge, H. Schneider, R. Barloutaud, P. Granet, J. Meyer, J.P. Porte; Phys. Letters 24B (1967) 198; Nuclear Physics B3 (1967) 592; see also Proceedings of the 1966 International Conference on High Energy Physics in Berkeley (page 183).

2. A.H. Rosenfeld, N. Barash-Schmidt, A. Barbaro-Galtieri, L.R. Price, P. Söding, C.G. Wohl, M. Roos, W.J. Willis; UCRL 8030 or Reviews of Modern Physics, January 1968.

3. A.H. Rosenfeld; Proceedings of the 1962 International Conference on High Energy Physics at CERN (page 325).

4. R.D. Tripp; CERN report 65-7 Rev. (1965) and Rendic. Scuola Internazionale di Fisica "E. Fermi", XXXIII Corso, (Academic Press, New York, page 70).

5. M. Alston, L.W. Alvarez, P. Eberhard, M.L. Good, W. Graziano, H.K. Ticho, S.G. Wojcicki; Phys. Rev. Letters 6, (1961) 300.

6. R.K. Böck, W.A. Cooper, B.R. French, J.B. Kinson, R. Levi-Setti, D. Revel, B. Tallini, S. Zylberajch; Phys. Letters 17, (1965) 166.

7. R.D. Tripp; Ann. Rev. Nucl. Sci. 15, (1965) 325.

8. G.A. Smith and J.S. Lindsey; Proc. of Athens Conf. on Resonant Particles (1965) 251.

9. M.B. Watson, M. Ferro-Luzzi, R.D. Tripp; Phys. Rev. 131, (1963) 2248.

10. J.D. Davies, J.D. Dowell, P.M. Hattersley, R.J. Homer, A.W. O'Dell, A.A. Carter, K.F. Riley, R.J. Tapper, D.V. Bugg, R.S. Gilmore, K.M. Knight, D.C. Salter, G.H. Stafford, E.J.N. Wilson; Phys. Rev. Letters 18, (1967) 62 and Rutherford Laboratory preprint RPP-H31 (1968).

11. CHS Collaboration, same authors as in ref. 1; Phys. Letters 19 (1965) 338.

12. CHS Collaboration, same authors as in ref. 1; private communication.

13. J.M. Blatt and V.F. Weisskopf; Theoretical Nuclear Physics (Wiley, New York 1952), page 361.

14. D. Berley, P.L. Connolly, E.L. Hart, D.C. Rahm, D.L. Stonehill, W.B. Thevenet, W.J. Willis, S.S. Yamamoto; Phys. Rev. Letters 15 (1965) 641.

15. R.H. Dalitz; Ann. Rev. Nucl. Sci. 13 (1963) 339.

16. W.M. Smart, A. Kernan, G.E. Kalmus, R.P. Ely; Phys. Rev. Letters 17 (1966) 556.
R.B. Bell, R.W. Birge, Y. Pan, R.T. Pu; Phys. Rev. Letters 16 (1966) 203.
S. Fenster, N.M. Gelfand, D. Harmsen, R. Levi-Setti, M. Raymond, J. Doede, W. Männer; Phys. Rev. Letters 17 (1966) 841.

17. A. Barbaro-Galtieri, A. Hussein and R.D. Tripp; Phys. Letters 6 (1963) 296.

18. J.K. Kim; Phys. Rev. Letters 19 (1967) 1074.

19. R.J. Abrams, R.L. Cool, G. Giacomelli, T.F. Kycia, B.A. Leontic, K.K. Li, D.N. Michael; Phys. Rev. Letters 19 (1967) 678.

20. C. Daum, F. Erné, J.P. Lagnaux, J.C. Sens, M. Steuer, F. Udo; Nuclear Physics (1968) in press and communication at the Heidelberg International Conference on High Energy Physics (1967).

21. C.G. Wohl, F.T. Solmitz and M.L. Stevenson; Phys. Rev. Letters 17 (1966) 107.

22. M.N. Focacci and G. Giacomelli; CERN report 66-18 (1966).

23. H. Steiner, UCRL-17903 (1967).

24. P. Bareyre, C. Bricman and G. Villet; Phys. Rev. 165 (1968) 1730 and private communication from C. Bricman.

25. A. Donnachie in Particle Interactions at High Energies; Scottish Universities' Summer School 1966 (Oliver and Boyd, London) page 330.

26. A. Donnachie, R.G. Kirsopp and C. Lovelace; Phys. Letters 26B (1968) 161 and C. Lovelace; rapporteur's talk at the 1967 Heidelberg Conference.

27. S. Glashow and A.H. Rosenfeld; Phys. Rev. Letters 10 (1963) 192. M. Goldberg, J. Leitner, R. Musto, L. O'Raifertaigh; Nuovo Cimento 49A (1966) 169.

28. CHS Collaboration, same authors as in ref. 1; Nuclear Physics B3 (1967) 10 and R.D. Tripp; review talk at the Coral Gables 1967 Conference (Freeman and Co., St. Francisco and London, 1967) page 237.

29. J.J. De Swart, Revs.Mod. Physics 35 (1963) 916.

30. P. McNamee and F. Chilton; Revs. Mod Physics 36 (1964) 1005.

31. A. Kernan and W.M. Smart; Phys. Rev. Letters 17 (1966) 832.